Retreat of Thwaites Glacier Triggered by its Neighbours

Matt Trevers[1], Stephen L Cornford[1], Antony J Payne[2], Edward Gasson[3], and Suzanne L Bevan[4]

[1]University of Bristol
[2]University of Liverpool
[3]University of Exeter
[4]Swansea University

March 04, 2024

Abstract

The Amundsen Sea Embayment in West Antarctica is experiencing the most rapid mass loss and grounding line retreat in Antarctica. Its glaciers are vulnerable to retreat through marine ice sheet instability. There is uncertainty over the timing and magnitude of retreat and in particular the response of Thwaites Glacier to thinning of its ice shelf and to ocean forced retreat of its neighbouring glaciers. We find that the response of Thwaites to melting of its ice shelf is limited. However, retreat of its neighbours can drive substantial retreat in Thwaites. We examine the impact of ice shelf buttressing on the stability of the grounding line. Further experiments show that extreme ice shelf forcings are required to trigger retreat in Thwaites in isolation. We also demonstrate that long-term stability is sensitive to the treatment of basal stress near the grounding line.

Retreat of Thwaites Glacier Triggered by its Neighbours

Matt Trevers[1], Stephen L. Cornford[1], Antony J. Payne[2], Edward Gasson[3], Suzanne Bevan[4]

[1]Centre for Polar Observation and Modelling, School of Geographical Sciences, University of Bristol, Bristol, UK
[2]School of Environmental Sciences, University of Liverpool, Liverpool, UK
[3]Centre for Geography and Environmental Sciences, University of Exeter, Cornwall, UK
[4]Department of Geography, Faculty of Science and Engineering, Swansea University, Swansea, UK

Key Points:

- Limited retreat of present-day Thwaites Glacier in response to submarine melting of its floating ice shelf
- Dynamical interactions with its neighbours can drive very rapid and substantial retreat in Thwaites
- Extreme ice shelf forcing scenarios or reduced basal stress near the grounding line can also drive widespread grounding line retreat

Corresponding author: Matt Trevers, matt.trevers@bristol.ac.uk

Abstract

The Amundsen Sea Embayment in West Antarctica is experiencing the most rapid mass loss and grounding line retreat in Antarctica. Its glaciers are vulnerable to retreat through marine ice sheet instability. There is uncertainty over the timing and magnitude of retreat and in particular the response of Thwaites Glacier to thinning of its ice shelf and to ocean forced retreat of its neighbouring glaciers. We find that the response of Thwaites to melting of its ice shelf is limited. However, retreat of its neighbours can drive substantial retreat in Thwaites. We examine the impact of ice shelf buttressing on the stability of the grounding line. Further experiments show that extreme ice shelf forcings are required to trigger retreat in Thwaites in isolation. We also demonstrate that long-term stability is sensitive to the treatment of basal stress near the grounding line.

Plain Language Summary

Glaciers of the Amundsen Sea Embayment in West Antarctica, including Thwaites Glacier, are discharging ice to the oceans and contributing to rising sea levels faster than anywhere else in Antarctica. Thwaites' ice shelf, a floating extension of the glacier, is likely to disintegrate over coming decades. There is disagreement over the impact this will have on the flow of upstream ice, with some recent studies suggesting that the ice shelf is already so weakened that its loss will not have any major consequence. In line with those studies, we find that over millennial timescales Thwaites is not strongly affected by ocean-driven melting of its ice shelf, except in extreme ocean circulation scenarios. However we find that interactions with neighbouring glaciers can trigger widespread retreat across the Amundsen Sea Embayment through previously unexplored feedback processes. We also find that Thwaites' long-term stability is dependent on the physics of the ice-bed interface. Our results demonstrate that individual Antarctic glaciers cannot be modelled as isolated systems, and highlight the need for an improved understanding of basal conditions and processes.

1 Introduction

The largest uncertainty in projections of global sea level rise (SLR) over the coming centuries is due to the contribution of the Antarctic Ice Sheet (Church et al., 2013). The fastest present-day mass loss is occurring in the Amundsen Sea Embayment (ASE) in West Antarctica (Shepherd et al., 2018). Thinning rates of several meters per year are observed for the ice shelves and grounding regions of the ASE (B. E. Smith et al., 2020) driven by strong ocean warming and sub-shelf melting (e.g. Naughten et al., 2022; Holland et al., 2023). The ASE is at risk of rapid grounding line retreat by marine ice sheet instability (MISI; Weertman, 1974; Schoof, 2007), which could potentially lead to collapse of the marine-based sectors of the West Antarctic Ice Sheet (WAIS) (Hughes, 1981; Feldmann & Levermann, 2015a). MISI can occur when the grounding line is positioned on a retrograde bed slope below sea level. Buttressing arising from lateral drag in confined ice shelves or pinning on ice rises beneath unconfined tongues can confer stability to grounded ice on a retrograde bed slope (e.g. Dupont & Alley, 2005; Goldberg et al., 2009; Favier & Pattyn, 2015). Ocean-forced thinning of ice shelves therefore has the potential to trigger grounding line retreat (R. B. Alley et al., 2015).

The configuration of the ASE ice streams, shelves and drainage basins is shown in Figure 1. The Crosson/Dotson (CD) basin contains the complex system of (from west to east) Kohler, Smith, Pope and Haynes glaciers discharging ice into the confined Dotson and Crosson ice shelves which branch around Bear Peninsula. The CD shelves and their tributary glaciers have seen thinning, acceleration and grounding line retreat in recent years (Lilien et al., 2018), with retreat rates of up to 11.7 km/year observed for Pope Glacier in 2017 (Milillo et al., 2022). This retreat is hypothesised to be driven by strong ice-ocean interactions in newly opened cavities.

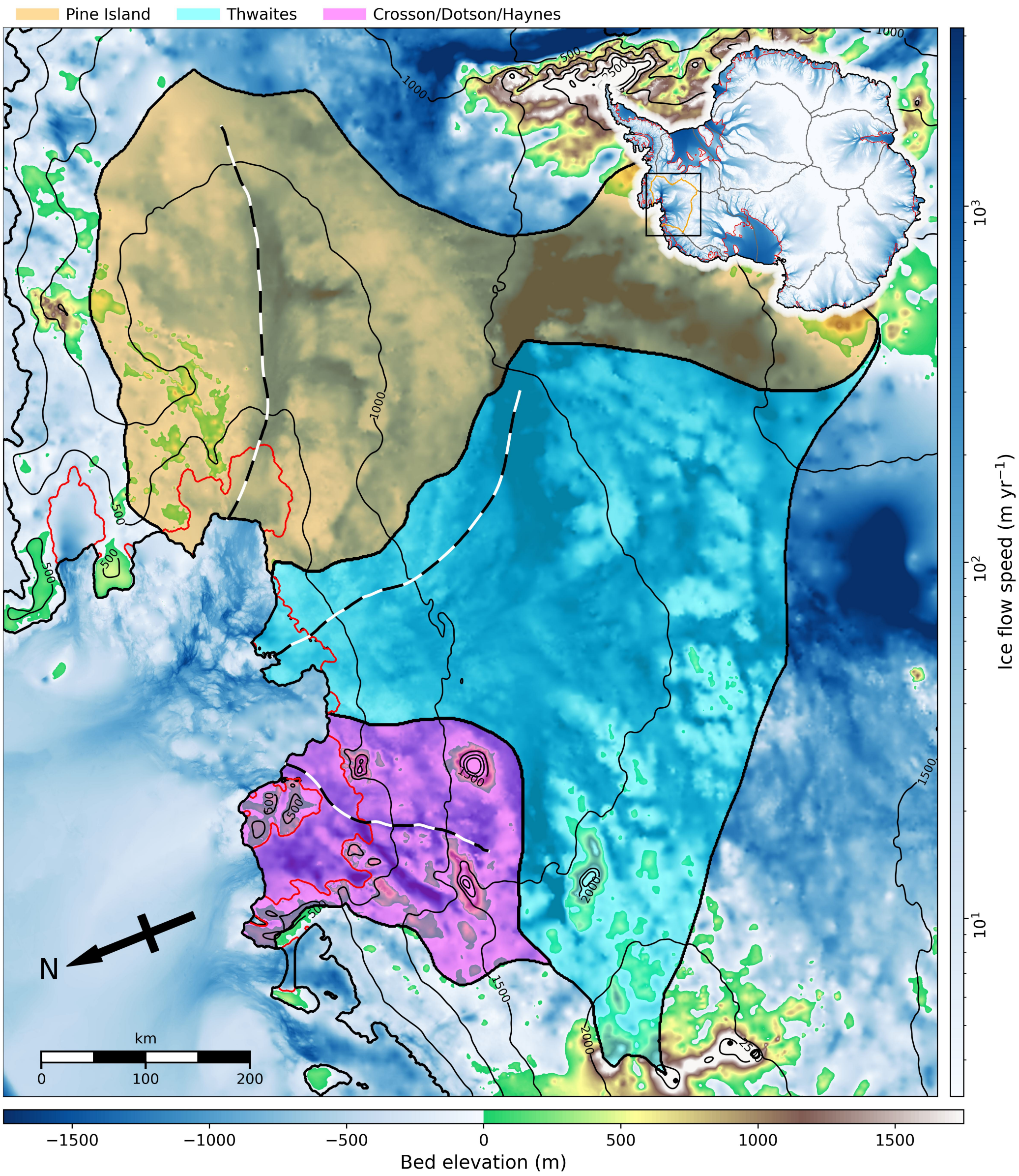

Figure 1. Bed topography of the ASE domain. Thick black lines show the initial ice front extent and basin boundaries, red lines the initial grounding line, thin black contours ice surface elevation and dashed black and white lines flowlines used in this study. Transparent shaded regions highlight individual glacier basins (Mouginot et al., 2017). The inset map shows Antarctic-wide flow speeds (Mouginot et al., 2019) with drainage boundaries from (Zwally et al., 2012). The black box shows the extent of the ASE domain within Antarctica.

Thwaites Glacier (TG) contains the sea level equivalent (SLE) of 0.6 m of ice and is one of the largest contributors to modern-day SLR (Holt et al., 2006). The grounding line retreated by 14 km from 1992 to 2011 (Rignot et al., 2014) and the mass loss rate increased by 22 Gt/year between 2006 and 2014 (Mouginot et al., 2014). The present-day grounding line is situated on a submarine ridge roughly 250 to 1000 m below sea level, with the bed rapidly deepening upstream. The TG ice shelf (TGIS) has undergone significant changes in recent decades (K. E. Alley et al., 2021). The TGIS is composed of the western ice tongue (TWIT) and the eastern ice shelf (TEIS) separated by a shear margin. TWIT detached from its pinning point around 2009 and rapidly disintegrated and accelerated (Miles et al., 2020). TEIS remains grounded on a pinning point near its ice front, confining TEIS and slowing ice flow relative to TWIT. TEIS initially accelerated following unpinning of TWIT but decelerated again as the shear margin weakened. The TEIS pinning point has progressively weakened due to thinning of TEIS since 2009 and may unpin entirely within a decade (Wild et al., 2022). Benn et al. (2022) suggested that backstress from the pinning point contributes to weakening and fracturing of TEIS as it thins.

Pine Island Glacier (PIG) is the single largest Antarctic contributor to SLR in recent decades (Rignot et al., 2019). It experienced significant 20th century retreat following ungrounding from a prominent seafloor ridge (J. A. Smith et al., 2017). Its present day grounding line is located in a constriction of the bed trough through which it discharges ice into its confined ice shelf (PIIS) (Reed et al., 2024). It has continued to thin and retreat in recent years (Mouginot et al., 2014; Rignot et al., 2019).

Both modelling and observational studies have suggested that MISI-driven retreat may already be underway for PIG and TG (e.g. Favier et al., 2014; Rignot et al., 2014; Mouginot et al., 2014; Joughin et al., 2014). More recent modelling studies have suggested a more limited SLR contribution by 2100, with the timing and magnitude of retreat sensitive to uncertain model parameters and the applied forcing (Yu et al., 2018; Alevropoulos-Borrill et al., 2020). Nias et al. (2016) found that unpinning of TEIS had negligible effect on the flow of grounded ice, while Benn et al. (2022) and Gudmundsson et al. (2023) both suggested that TEIS has limited buttressing impact and that its loss would be unlikely to trigger significantly increased ice discharge from TG.

A number of studies have demonstrated that dynamical interactions between neighbouring basins can significantly effect projected mass loss rates (Feldmann & Levermann, 2015a, 2015b; Martin et al., 2019). However ice sheet models commonly model isolated basins to limit the computational cost (e.g. Favier et al., 2014; Joughin et al., 2014; Seroussi et al., 2017) or whole ice sheets at reduced resolution (e.g. Feldmann & Levermann, 2015a; Golledge et al., 2015; DeConto et al., 2021). In this study we examine interbasin interactions within the ASE and their dynamical impact on the evolution of the individual basins over millennial timescales. We find that TG retreat can be driven by the evolution of its neighbours and we explore the mechanisms driving the interactions. We conduct an analysis of the buttressing strength for different configurations of the TG ice shelf and grounding line. Further experiments apply enhanced forcings to test the limits of TG's grounding line stability.

2 Methods

We used the BISICLES adaptive mesh refinement (AMR) ice flow model (Cornford et al., 2013). The AMR functionality enables mesh resolution of 500 m at the grounding line in concert with coarser resolution of 4 km for inland ice. A modern-day ASE initial condition comprising consistent fields of basal friction coefficient C, ice stiffening factor ϕ and a relaxed surface geometry was derived through an iterative procedure which follows Bevan et al. (2023); van den Akker et al. (2023) and which is detailed in Supporting Text S1. BedMachine v3 (Morlighem et al., 2020; Morlighem, 2022) provided bed topography and pre-initialisation ice geometry. Non-evolving surface accumulation rates came from the 1980 to 2021 mean of the MAR regional climate model (Agosta et al., 2019). The three dimensional temperature field was generated by a thermal spin-up which is described in Supporting Text S2. Model inputs are shown in Figure S3.

We carried out two sets of experiments, detailed separately below. The first set of experiments, described in Section 2.1, explore the dynamical interactions between drainage basins in the ASE. The second set, described in Section 2.2, apply a range of enhanced forcings to TG in isolation.

2.1 Interbasin Interactions

These experiments explored the response of the ASE to the focused regional application of basal melt, and the interactions between drainage basins. Sub-ice shelf melt was applied for 1000 years to the isolated PIG, TG and CD basins, the combinations of PIG+TG and CD+TG, and finally to all three basins combined. We applied the depth-dependent melt rate parameterisation described in Supporting Text S3 which reached a maximum of 250 m/year at a depth of 1000 m.

Basal stress for grounded ice was determined by a Regularised Coulomb friction law,

$$\boldsymbol{\tau}_{b,r} = -C\,|\boldsymbol{u}_b|^{m-1}\left(\frac{|\boldsymbol{u}_b|}{u_0}+1\right)^{-m}\cdot\boldsymbol{u}_b, \tag{1}$$

where C is the spatially varying friction coefficient, $\boldsymbol{u}_b$ the basal sliding velocity, $m = 1/3$ the friction law exponent and $u_0 = 50$ m/year the fast sliding speed. This expression is equivalent to that introduced by Joughin et al. (2019). A variable calving rate was applied at the ice front anti-parallel to the direction of ice flow,

$$\boldsymbol{u}_c = -r_c\cdot\boldsymbol{u}_T, \tag{2}$$

where $\boldsymbol{u}_T$ is the terminus velocity and r_c the constant calving multiplier. We set $r_c = 1$ to prohibit ice front advance, while retreat can still result from thinning.

Results and discussion of these experiments are presented in Section 3.1, along with an analysis of the buttressing strength for different configurations of the TG ice shelf and grounding line. Animated plots of all experiments in this section are provided with the supplementary material.

2.2 Thwaites Enhanced Forcings

In these experiments a range of enhanced forcings were applied to TG in order to probe the limits of stability of its grounding line. Experiments were continued from the final state after 1000 years of the TG melt experiment described in Section 2.1.

Sub-ice shelf melt was applied for a further 1000 years to the TG basin. Four sets of enhanced forcings were applied: (1) The depth-dependent melt rate described in Supporting Text S3 with a range of maximum values up to 2000 m/year at 1000 m depth. (2) Melting was applied uniformly across the ice shelf independent of depth, with a range of melt rates up to 1250 m/year. (3) Enhanced calving via a range of additional calving multipliers applied to floating ice in the TG basin with a draft of less than 100 m. (4) Application of an alternative Coulomb-limited friction law introduced by Tsai et al. (2015),

$$\boldsymbol{\tau}_{b,T} = -\frac{\boldsymbol{u}_b}{|\boldsymbol{u}_b|}\cdot\min\left[|\boldsymbol{\tau}_{b,r}|\,,\alpha N\right], \tag{3}$$

where $\alpha = 0.5$ is a dimensionless coefficient and N is the basal effective pressure. $\boldsymbol{\tau}_{b,r}$ was calculated from Equation 1. This expression, referred to as the Tsai law from hereon in, prohibits the basal stress from exceeding the effective pressure.

For all enhanced forcing experiments, model parameters from Section 2.1 were applied unless otherwise specified. Results and discussion of the response of TG to these enhanced forcings are presented in Section 3.2.

3 Results and Discussion

3.1 Interbasin Interactions

Figure 2 shows a contrast in the response of PIG and TG to melting of their ice shelves. Melting of PIIS lead to almost complete deglaciation of the marine-based parts of PIG within 1000 years, and complete or ongoing deglaciation of TG. PIG retreated in every experiment in which it was subjected to the melt forcing (dashed lines, Panel f). It retreated earlier than TG and at an almost identical rate between experiments, indicating that its retreat is unaffected by its neighbour. By contrast, TG did not retreat significantly when TGIS was melted in isolation (orange lines), with its grounding line restabilising a few tens of kilometers upstream of its initial position. Instead retreat of PIG was necessary to trigger more substantial retreat in TG. The retreat and thinning of PIG drove significant drawdown of ice from TG, seen as a large ice flux across the basin boundary (blue line, Panel g). This enhanced thinning of inland ice in TG drove retreat of its grounding line, which accelerated once it had retreated over deeper bed. Applying melt simultaneously to both basins (cyan lines) triggered earlier retreat in TG due to thinning from the combination of sources. The resulting simultaneous retreat in both basins lead to ice fluxes in alternating directions across the dividing boundary at different times (Panel g). At 525 years ASE mass loss peaked at $\sim$7 mm/year SLE, an order of magnitude faster than the current observed mass loss rate for the entire ice sheet (B. E. Smith et al., 2020). Grounding line retreat rates in TG peaked at $\sim$7 km/year which is within the observed range of retreat rates Milillo et al. (2022). Applying melt in all ASE basins (red lines) produced very similar patterns of mass loss, with retreat in TG triggered 50 years earlier.

Figure 3 shows the interactions between the CD and TG basins. With melt applied in isolation CD saw limited retreat, with its grounding line eventually restabilising in a retreated position up to $\sim$100 km upstream. Thinning in CD drove drawdown from TG across the dividing boundary (blue line, Panel g), but the associated thinning in TG wasn't sufficient to trigger retreat there. With melt was also applied to TG, the boundary ice flux into CD was initially smaller since TG was also thinning (cyan line, Panel g). The reduced inflow from TG drove further retreat in CD (Panel b), in turn driving increased inflow from TG after 325 years. The enhanced thinning of TG eventually lead to very rapid retreat of the TG grounding line (Panel f) and widespread deglaciation in both basins (Panels c, d).

Martin et al. (2019) demonstrated the importance of ice-dynamical interactions between basins at the regional scale. They found a modest increase in the rate of mass loss after $\sim$100 years when ASE melting was combined with melting in either the Eastern Ross Sector (including the Siple Coast ice streams) or the Western Ronne sector, as compared with the summed mass loss when melt was applied separately. Similarly, Feldmann and Levermann (2015a) showed that thinning and retreat in the ASE could cause migration of the upstream ice divide into the Ross and Filcher-Ronne drainage basins, ultimately triggering collapse in those basins after several thousand years. By contrast, interbasin interactions in our experiments drove significantly increased discharge within a few hundred years and could trigger collapse of the CD and TG basins within a thousand years. The interacting basins in our experiments are side-by-side neighbours with ice flowing parallel to dividing boundaries, thus flow reorganization can occur rapidly after the onset of retreat. In the earlier studies interactions occurred across the upstream ice divide, hence with a significant lag following the onset of ocean-driven thinning.

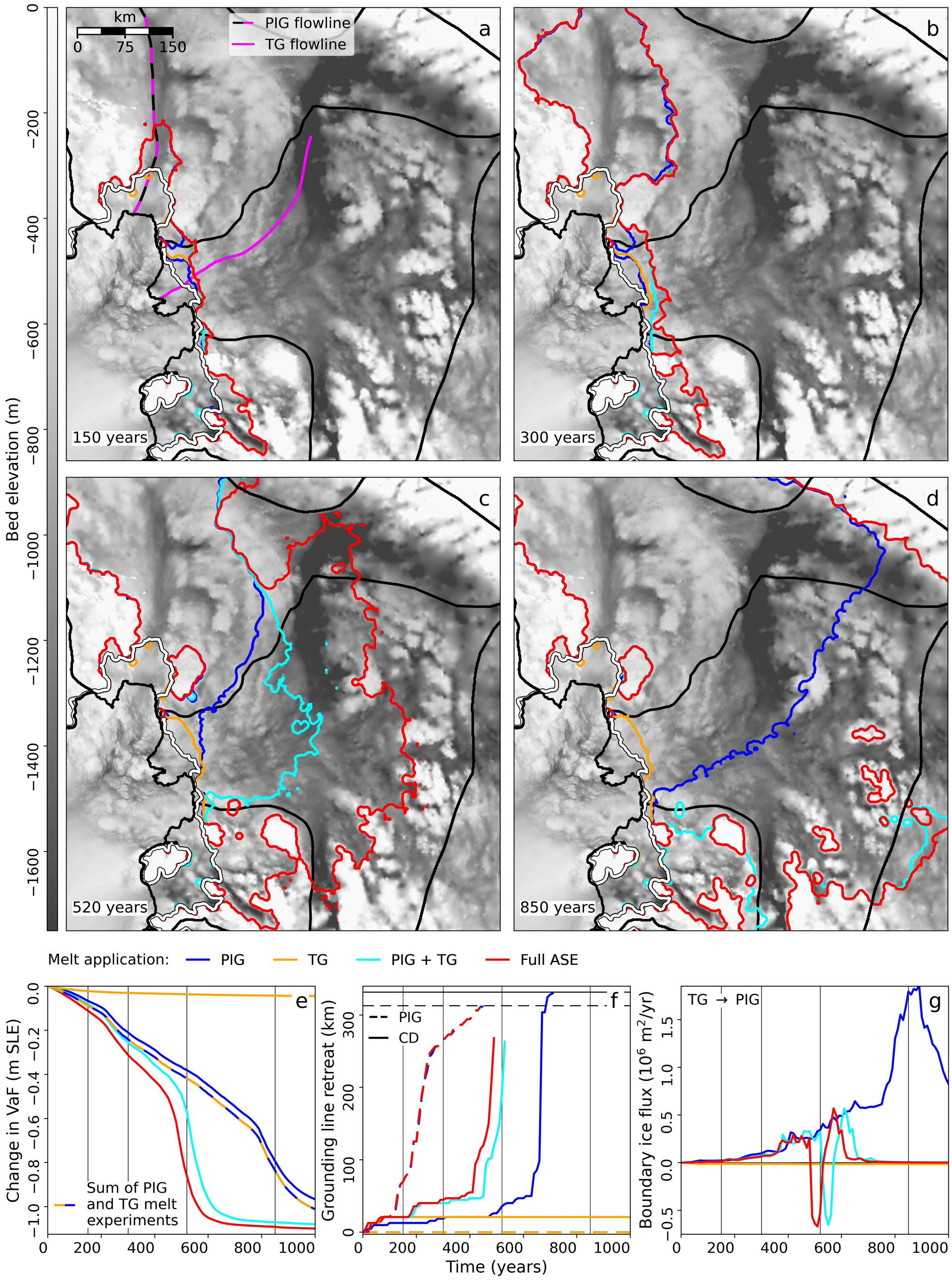

Figure 2. Maps and timeseries of the ASE evolution for PIG, TG, combined PIG+TG and full ASE melt experiments. (a) to (d) Grounding lines for all experiments (coloured lines) at selected snapshots. Also shown are the basin boundaries and initial ice front (black lines) and initial grounding lines (white lines with black edges). Panel (a) also shows PIG and TG flowlines. (e) Change in ASE Volume above Flotation (VaF), including the summed VaF change of the individual PIG and TG melt experiments. (f) Grounding line retreat in PIG (dashed lines) and TG (solid lines). Lines are truncated where the grounding line retreats beyond the end of the flowline. Black horizontal lines show the flowline extents in PIG and TG respectively. Note that blue, cyan and red dashed lines overlap. (g) Ice thickness flux per unit length across the PIG-TG basin boundary, defined such that positive flux refers to flow out of the TG basin. Vertical black lines in (e) to (g) refer to panels (a) to (d).

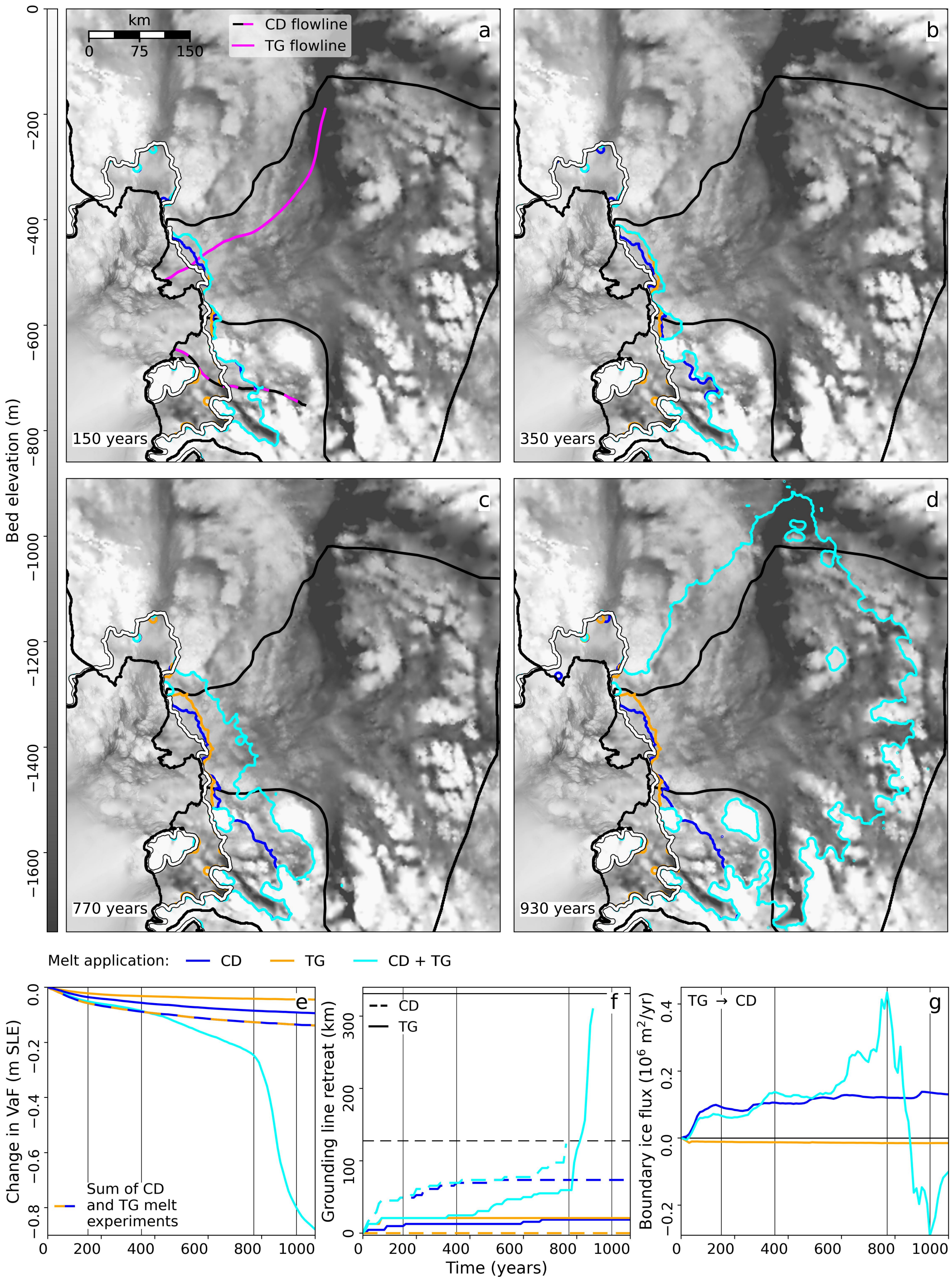

Figure 3. Maps and timeseries plots of the evolution of the ASE for CD, TG and combined CD+TG melt experiments. (a) to (g) as for Figure 2, except that the dashed blue and orange line in (e) shows the summed VaF loss from individual CD and TG melt experiments, dashed lines in (f) refer to the CD basin and fluxes in (g) are measured across the CD-TG basin boundary.

Gudmundsson et al. (2023) conducted an analysis of the strength of ice shelf buttressing in the ASE. They showed that TGIS provides limited buttressing compared with the PIG and CD shelves, and that much of the buttressing provided by TGIS could be explained by the small-scale embayments in the grounding line. We conduct a similar analysis by computing the buttressing number θ_n, the ratio of the resistive stress across the grounding line to the resistive stress in the absence of an ice shelf. The formulation of the buttressing number is described in Supporting Text S4. By definition $\theta_n = 1$ where there is zero buttressing. The ice shelf provides buttressing where $\theta_n < 1$, *anti-buttressing* where $\theta_n > 1$ and *super-buttressing* where $\theta_n < 0$. Figure S4 shows buttressing numbers calculated for TG grounding lines at the start and end of the isolated TG melt experiment (orange lines, Figure 2). Both configurations follow elevated features of the underlying bed. Local embayments were more heavily buttressed while convexities were often unbuttressed or even anti-buttressed. The histogram shows that the buttressing strength in the final configuration decreased relative to the initial state, indicating that grounding line stability was less dependent on the integrity of TGIS. Nonetheless, the final grounding line still contains some localised strongly buttressed regions which might be vulnerable to further degradation of TGIS. In three highlighted locations, the proximity of buttressed embayments in the final grounding line to overdeepened channels leading to the basin interior provide potential pathways to rapid retreat and deglaciation.

We studied the impact of unpinning TEIS by reducing the basal friction coefficient beneath the pinning point to zero in a diagnostic setting (Figure S5). This produced a significant instantaneous speedup for floating ice, but the speedup for grounded ice was limited to between 10 and 30% in a region within 25 km of the grounding line, focused on an anti-buttressed grounded protrusion. There was a minor reduction in the buttressing strength at the grounding line. A secondary pinning point located just downstream of the grounding line was found to have negligible impact on buttressing or the flow of TEIS. This demonstrates that while the pinning point constrains the flow of ice in TEIS, its buttressing effect on grounded ice is limited due to the highly fractured nature of TEIS. We find agreement with Benn et al. (2022) and Nias et al. (2016) who showed that unpinning of TEIS would have little impact on the discharge of grounded ice and is unlikely to immediately trigger marine ice sheet instability, although both studies used the same ice flow code as in this study. Wild et al. (2022) similarly found that ungrounding of TEIS produced only a 10% speedup across the grounding line.

3.2 Thwaites Enhanced Forcings

In Section 3.1 we showed that TG is not strongly sensitive to melting of its own ice shelf, with the grounding line restabilising a few tens of kilometers upstream. Additional thinning of upstream grounded ice driven by interactions with neighbouring glaciers was required to trigger more substantial retreat. The experiments in this section aim to establish whether TG is always resistant to standalone forcing.

Figure 4 shows the TG grounding line retreat in response to the enhanced forcings described in Section 2.2. These additional forcings were able to trigger substantial retreat in the TG basin, with more aggressive forcings producing earlier retreat. Retreat followed a similar pattern in all cases, with gradual retreat in short sporadic episodes until a final quasi-stable position was reached at 34 km. Further retreat from this position initiated rapid retreat as the bed deepens steeply upstream (Morlighem et al., 2020). The rate of retreat slowed again across a region between $\sim$75 and $\sim$125 km upstream before very rapid retreat was re-established, resulting in widespread deglaciation across the TG basin. Retreat rates peaked between 5 and 10 km/year during the most rapid phase of retreat (Figure S6). Figure S7 shows that the different types of forcing produced similar patterns of retreatt. Retreat tended to originate at the orange-highlighted embayment in Figure S4 and followed overdeepened channels cutting through the elevated bed region before reaching deeper bedrock further upstream. This demonstrates that de-

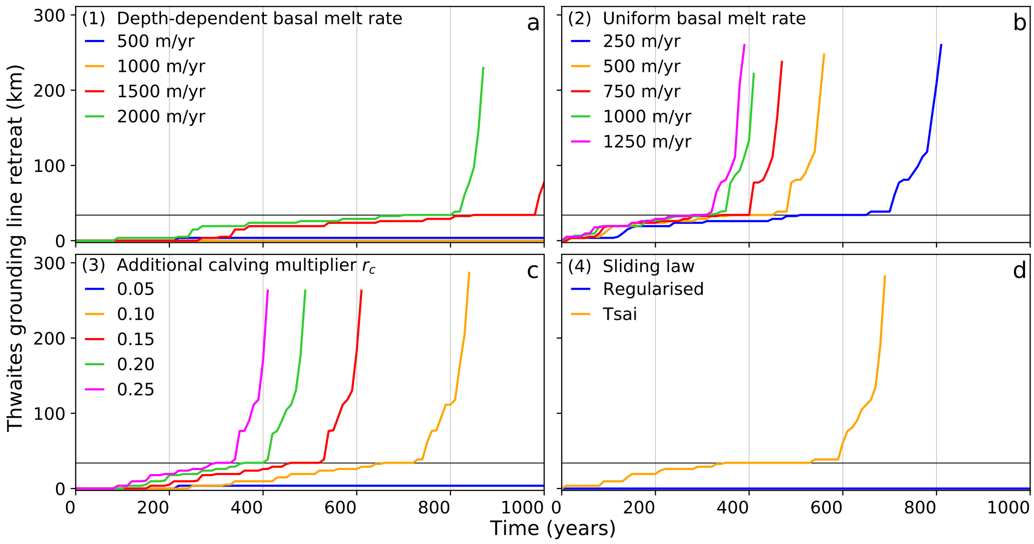

Figure 4. Grounding line retreat along the TG flowline for enhanced forcing experiments. Lines are truncated where the grounding line retreats beyond the end of the flowline, with the vertical scale covering the full flowline extent. Horizontal lines are drawn at 34 km.

spite TGIS being largely passive, localised remnant ice shelf embayments can still produce significant buttressing and their continued degradation can destabilise vulnerable portions of the grounding line. We stress that these enhanced melt rates are much higher than could be expected under modern conditions and are intended to establish the limits of stability.

A depth-dependent melt rate peaking at 1500 m/year at 1000 m depth (red line, Panel a) was required to trigger substantial retreat, whereas only 250 m/year of uniform melting (blue line, Figure 4b) triggered earlier retreat. The 1500 m/year depth-dependent melt forcing produced 572 Gt/year of melt across TGIS at the start of the experiment whereas the 250 m/year uniform melt forcing produced more melt at 684 Gt/year. The enhanced calving experiments (Panel c) produced similarly timed retreat to the uniform melt rates. The resulting calving rates which peak at 125 % of the shelf front velocity are seemingly within a realistic range (e.g. DeConto et al., 2021). However it should be noted that the calving rate forcing was designed to produce continual degradation of the ice shelf, and therefore unlike for the melt forcings it was impossible for the ice shelf to reach a balanced equilibrium with the calving rate.

Limiting the basal stress to the effective pressure with the application of the Tsai Law (Panel d, Equation 3) lowered the basal stress within a few kilometers upstream of the grounding line, triggering an instantaneous speedup of up to 500 m/year (Figure S8). This drove additional dynamic thinning, episodic grounding line retreat and further acceleration, eventually leading to rapid widespread retreat after 600 years. This sensitivity to the choice of sliding law reflects our uncertainty and lack of knowledge of basal condition, sliding mechanisms and grounding processes (e.g. Parizek et al., 2013; Joughin et al., 2019; Zoet & Iverson, 2020). Ice flow models commonly assume a discrete grounding line representing an abrupt transition from grounded ice upstream to floating ice downstream. In reality there is a less clearly defined grounding zone with variable grounding strength, driven by tidal motion (e.g. Ciracì et al., 2023). Walker et al. (2013) showed that tidal flexure of ice shelves could cause low tide uplift at centimeter scales a few kilometers upstream of the grounding line, with the possibility for seawater intrusions, while

Milillo et al. (2022) observed grounding zones up to 3 km in width for Pope, Smith and Kohler glaciers. Parizek et al. (2013) inferred the possibility of seawater influence up to 10 km inland from the grounding line. They showed that incorporating a grounding zone with decreased basal friction into a model of TG was able to trigger retreat. The reduction in basal stress generated by the Tsai law in our experiments occurred across similar distances upstream of the grounding line, creating an effective grounding zone. Our results therefore support their conclusions.

4 Conclusions

We have demonstrated that the dynamical interactions between neighbouring basins are a crucial component of the evolution of the ASE, and therefore important in assessing the stability of WAIS. TG was resistant to melting of TGIS in isolation, and required additional thinning generated by simultaneous melting of its neighbours to trigger substantial retreat. By contrast retreat of PIG was easily triggered and dominated the dynamics of its neighbours. We explored the limits of stability of TG and found that further degradation of TGIS through extreme melting or enhanced calving could tip the glacier into retreat. Our results provide further evidence that the present-day TGIS provides limited stability to the grounded glacier (e.g. Benn et al., 2022; Gudmundsson et al., 2023), but localised remnant ice shelf embayments can still produce sufficient buttressing to halt further retreat. An alternative sliding law mimicking a grounding zone with reduced ice-bed contact also produced rapid retreat after several centuries. Our study demonstrates that for projections beyond decadal timescales, individual glacier basins of WAIS cannot be considered as isolated systems. We also highlight the importance of improved model implementations of sliding processes and grounding zone conditions to inform more accurate projections of ice sheet evolution over coming centuries.

Open Research Section

The BISICLES ice sheet model is open source and is available for download from https://github.com/ggslc/bisicles-uob. The data on which this study is based are available in Mouginot et al. (2017), Agosta et al. (2019), Mouginot et al. (2019), Burton-Johnson et al. (2020), B. E. Smith et al. (2020) and Morlighem (2022). We did not generate any new observational data products.

Acknowledgments
The authors gratefully acknowledge helpful discussions with Paul Holland and Kaitlin Naughten. This research was carried out as part of the NSFGEO-NERC Pliocene sea level amplitudes (PLIOAMP) project (NE/T007397/1). MT was also partly funded by the UK NERC Centre for Polar Observation and Modelling (CPOM). This work used the ARCHER2 UK National Supercomputing Service (https://www.archer2.ac.uk) and the computational facilities of the Advanced Computing Research Centre, University of Bristol (http://www.bristol.ac.uk/acrc/).

References

Agosta, C., Amory, C., Kittel, C., Orsi, A., Favier, V., Gallée, H., ... Fettweis, X. (2019). Estimation of the Antarctic surface mass balance using the regional climate model MAR (1979–2015) and identification of dominant processes. *The Cryosphere*, *13*(1), 281–296. doi: 10.5194/tc-13-281-2019

Alevropoulos-Borrill, A. V., Nias, I. J., Payne, A. J., Golledge, N. R., & Bingham, R. J. (2020). Ocean-forced evolution of the Amundsen Sea catchment, West Antarctica, by 2100. *Cryosphere*, *14*(4), 1245–1258. doi: 10.5194/tc-14-1245-2020

Alley, K. E., Wild, C. T., Luckman, A., Scambos, T. A., Truffer, M., Pettit, E. C., . . . Dunmire, D. (2021). Two decades of dynamic change and progressive destabilization on the Thwaites Eastern Ice Shelf. *The Cryosphere*, *15*(11), 5187–5203. doi: 10.5194/tc-15-5187-2021

Alley, R. B., Anandakrishnan, S., Christianson, K., Horgan, H. J., Muto, A., Parizek, B. R., . . . Walker, R. T. (2015). Oceanic Forcing of Ice-Sheet Retreat: West Antarctica and More. *Annual Review of Earth and Planetary Sciences*, *43*(1), 207–231. doi: 10.1146/annurev-earth-060614-105344

Benn, D. I., Luckman, A., Åström, J. A., Crawford, A. J., Cornford, S. L., Bevan, S. L., . . . Bassis, J. (2022, jun). Rapid fragmentation of Thwaites Eastern Ice Shelf. *The Cryosphere*, *16*(6), 2545–2564. doi: 10.5194/tc-16-2545-2022

Bevan, S., Cornford, S. L., Gilbert, L., Otosaka, I., Martin, D., & Surawy-Stepney, T. (2023). Amundsen Sea Embayment ice-sheet mass-loss predictions to 2050 calibrated using observations of velocity and elevation change. *Journal of Glaciology*, 1–11. doi: 10.1017/jog.2023.57

Burton-Johnson, A., Dziadek, R., & Martin, C. (2020). Review article: Geothermal heat flow in Antarctica: current and future directions. *The Cryosphere*, *14*(11), 3843–3873. doi: 10.5194/tc-14-3843-2020

Church, J. A., Clark, P. U., Cazenave, A., Gregory, J. M., Jevrejeva, S., Levermann, A., . . . Unnikrishnan, A. A. (2013). Sea Level Change. In V. B. Stocker, T.F., D. Qin, G.-K. Plattner, M. Tignor, S.K. Allen, J. Boschung, A. Nauels, Y. Xia & P. Midgley (Eds.), *Climate change 2013: The physical science basis. contribution of working group i to the fifth assessment report of the intergovernmental panel on climate change* (pp. 1137–1216). Cambridge: Cambridge University Press. doi: 10.1017/CBO9781107415324.026

Ciracì, E., Rignot, E., Scheuchl, B., Tolpekin, V., Wollersheim, M., An, L., . . . Dini, L. (2023). Melt rates in the kilometer-size grounding zone of Petermann Glacier, Greenland, before and during a retreat. *Proceedings of the National Academy of Sciences*, *120*(20), 1–9. doi: 10.1073/pnas.2220924120

Cornford, S. L., Martin, D. F., Graves, D. T., Ranken, D. F., Le Brocq, A. M., Gladstone, R. M., . . . Lipscomb, W. H. (2013, jan). Adaptive mesh, finite volume modeling of marine ice sheets. *Journal of Computational Physics*, *232*(1), 529–549. doi: 10.1016/j.jcp.2012.08.037

DeConto, R. M., Pollard, D., Alley, R. B., Velicogna, I., Gasson, E., Gomez, N., . . . Dutton, A. (2021). The Paris Climate Agreement and future sea-level rise from Antarctica. *Nature*, *593*(7857), 83–89. doi: 10.1038/s41586-021-03427-0

Dupont, T. K., & Alley, R. B. (2005). Assessment of the importance of ice-shelf buttressing to ice-sheet flow. *Geophysical Research Letters*, *32*(4), 1–4. doi: 10.1029/2004GL022024

Favier, L., Durand, G., Cornford, S. L., Gudmundsson, G. H., Gagliardini, O., Gillet-Chaulet, F., . . . Le Brocq, A. M. (2014, feb). Retreat of Pine Island Glacier controlled by marine ice-sheet instability. *Nature Climate Change*, *4*(2), 117–121. doi: 10.1038/nclimate2094

Favier, L., & Pattyn, F. (2015, jun). Antarctic ice rise formation, evolution, and stability. *Geophysical Research Letters*, *42*(11), 4456–4463. doi: 10.1002/2015GL064195

Feldmann, J., & Levermann, A. (2015a). Collapse of the West Antarctic Ice Sheet after local destabilization of the Amundsen Basin. *Proceedings of the National Academy of Sciences*, *112*(46), 14191–14196. doi: 10.1073/pnas.1512482112

Feldmann, J., & Levermann, A. (2015b, apr). Interaction of marine ice-sheet instabilities in two drainage basins: simple scaling of geometry and transition time. *The Cryosphere*, *9*(2), 631–645. doi: 10.5194/tc-9-631-2015

Goldberg, D., Holland, D. M., & Schoof, C. (2009). Grounding line movement and ice shelf buttressing in marine ice sheets. *Journal of Geophysical Research: Earth Surface*, *114*(F4), 1–23. doi: 10.1029/2008JF001227

Golledge, N. R., Kowalewski, D. E., Naish, T. R., Levy, R. H., Fogwill, C. J., & Gasson, E. G. W. (2015). The multi-millennial Antarctic commitment to future sea-level rise. *Nature*, *526*(7573), 421–425. doi: 10.1038/nature15706

Gudmundsson, G. H., Barnes, J. M., Goldberg, D. N., & Morlighem, M. (2023). Limited Impact of Thwaites Ice Shelf on Future Ice Loss From Antarctica. *Geophysical Research Letters*, *50*(11), 1–11. doi: 10.1029/2023gl102880

Holland, P. R., Bevan, S. L., & Luckman, A. J. (2023). Strong Ocean Melting Feedback During the Recent Retreat of Thwaites Glacier. *Geophysical Research Letters*, *50*, 1–11. doi: 10.1029/2023GL103088

Holt, J. W., Blankenship, D. D., Morse, D. L., Young, D. A., Peters, M. E., Kempf, S. D., ... Corr, H. F. J. (2006, may). New boundary conditions for the West Antarctic Ice Sheet: Subglacial topography of the Thwaites and Smith glacier catchments. *Geophysical Research Letters*, *33*(9), 2–5. doi: 10.1029/2005GL025561

Hughes, T. J. (1981). The weak underbelly of the West Antarctic ice sheet. *Journal of Glaciology*, *27*(97), 518–525. doi: 10.3189/S002214300001159X

Joughin, I., Smith, B. E., & Medley, B. (2014). Marine Ice Sheet Collapse Potentially Under Way for the Thwaites Glacier Basin, West Antarctica. *Science*, *344*(6185), 735–738. doi: 10.1126/science.1249055

Joughin, I., Smith, B. E., & Schoof, C. (2019). Regularized Coulomb Friction Laws for Ice Sheet Sliding: Application to Pine Island Glacier, Antarctica. *Geophysical Research Letters*, *46*, 4764–4771. doi: 10.1029/2019GL082526

Lilien, D. A., Joughin, I., Smith, B. E., & Shean, D. E. (2018, apr). Changes in flow of Crosson and Dotson ice shelves, West Antarctica, in response to elevated melt. *The Cryosphere*, *12*(4), 1415–1431. doi: 10.5194/tc-12-1415-2018

Martin, D. F., Cornford, S. L., & Payne, A. J. (2019). Millennial-Scale Vulnerability of the Antarctic Ice Sheet to Regional Ice Shelf Collapse. *Geophysical Research Letters*, *46*(3), 1467–1475. doi: 10.1029/2018GL081229

Miles, B. W. J., Stokes, C. R., Jenkins, A., Jordan, J. R., Jamieson, S. S. R., & Gudmundsson, G. H. (2020). Intermittent structural weakening and acceleration of the Thwaites Glacier Tongue between 2000 and 2018. *Journal of Glaciology*, *66*(257), 485–495. doi: 10.1017/jog.2020.20

Milillo, P., Rignot, E., Rizzoli, P., Scheuchl, B., Mouginot, J., Bueso-Bello, J. L., ... Dini, L. (2022). Rapid glacier retreat rates observed in West Antarctica. *Nature Geoscience*, *15*(1), 48–53. doi: 10.1038/s41561-021-00877-z

Morlighem, M. (2022). *MEaSUREs BedMachine Antarctica, Version 3 [Data Set].* Retrieved 01-29-2024, from `https://nsidc.org/data/nsidc-0756/versions/3` doi: https://doi.org/10.5067/FPSU0V1MWUB6

Morlighem, M., Rignot, E., Binder, T., Blankenship, D., Drews, R., Eagles, G., ... Young, D. A. (2020). Deep glacial troughs and stabilizing ridges unveiled beneath the margins of the Antarctic ice sheet. *Nature Geoscience*, *13*(2), 132–137. doi: 10.1038/s41561-019-0510-8

Mouginot, J., Rignot, E., & Scheuchl, B. (2014). Sustained increase in ice discharge from the Amundsen Sea Embayment, West Antarctica, from 1973 to 2013. *Geophysical Research Letters*, *41*(5), 1576–1584. doi: 10.1002/2013GL059069

Mouginot, J., Rignot, E., & Scheuchl, B. (2019). *MEaSUREs Phase-Based Antarctica Ice Velocity Map, Version 1 [Data Set].* Retrieved 2024-01-29, from `https://nsidc.org/data/nsidc-0754/versions/1` doi: https://doi.org/10.5067/PZ3NJ5RXRH10

Mouginot, J., Scheuchl, B., & Rignot, E. (2017). *MEaSUREs Antarctic Boundaries for IPY 2007-2009 from Satellite Radar, Version 2 [Data Set].* Retrieved 2024-01-29, from `https://nsidc.org/data/nsidc-0709/versions/2` doi: https://doi.org/10.5067/AXE4121732AD

Naughten, K. A., Holland, P. R., Dutrieux, P., Kimura, S., Bett, D. T., & Jenkins, A. (2022). Simulated Twentieth-Century Ocean Warming in the

Amundsen Sea, West Antarctica. *Geophysical Research Letters*, *49*. doi: 10.1029/2021GL094566

Nias, I. J., Cornford, S. L., & Payne, A. J. (2016). Contrasting the modelled sensitivity of the Amundsen Sea Embayment ice streams. *Journal of Glaciology*, *62*, 552–562. doi: 10.1017/jog.2016.40

Parizek, B. R., Christianson, K., Anandakrishnan, S., Alley, R. B., Walker, R. T., Edwards, R. A., . . . Nowicki, S. M. J. (2013). Dynamic (in)stability of Thwaites Glacier, West Antarctica. *Journal of Geophysical Research: Earth Surface*, *118*(2), 638–655. doi: 10.1002/jgrf.20044

Reed, B., Green, J. A. M., Jenkins, A., & Gudmundsson, G. H. (2024). Recent irreversible retreat phase of Pine Island Glacier. *Nature Climate Change*, *14*(1), 75–81. doi: 10.1038/s41558-023-01887-y

Rignot, E., Mouginot, J., Morlighem, M., Seroussi, H., & Scheuchl, B. (2014). Widespread, rapid grounding line retreat of Pine Island, Thwaites, Smith, and Kohler glaciers, West Antarctica, from 1992 to 2011. *Geophysical Research Letters*, *41*(10), 3502–3509. doi: 10.1002/2014GL060140

Rignot, E., Mouginot, J., Scheuchl, B., van den Broeke, M., van Wessem, M. J., & Morlighem, M. (2019). Four decades of Antarctic Ice Sheet mass balance from 1979–2017. *Proceedings of the National Academy of Sciences*, *116*(4), 1095–1103. doi: 10.1073/pnas.1812883116

Schoof, C. (2007, sep). Ice sheet grounding line dynamics: Steady states, stability, and hysteresis. *Journal of Geophysical Research: Earth Surface*, *112*(F3), F03S28. doi: 10.1029/2006JF000664

Seroussi, H., Nakayama, Y., Larour, E., Menemenlis, D., Morlighem, M., Rignot, E., & Khazendar, A. (2017). Continued retreat of Thwaites Glacier, West Antarctica, controlled by bed topography and ocean circulation. *Geophysical Research Letters*, *44*(12), 6191–6199. doi: 10.1002/2017GL072910

Shepherd, A., Ivins, E., Rignot, E., Smith, B. E., van den Broeke, M. R., Velicogna, I., . . . Wouters, B. (2018). Mass balance of the Antarctic Ice Sheet from 1992 to 2017. *Nature*, *558*(7709), 219–222. doi: 10.1038/s41586-018-0179-y

Smith, B. E., Fricker, H. A., Gardner, A. S., Medley, B., Nilsson, J., Paolo, F. S., . . . Zwally, H. J. (2020). Pervasive ice sheet mass loss reflects competing ocean and atmosphere processes. *Science*, *368*(6496), 1239–1242. doi: 10.1126/science.aaz5845

Smith, J. A., Andersen, T. J., Shortt, M., Gaffney, A. M., Truffer, M., Stanton, T. P., . . . Vaughan, D. G. (2017). Sub-ice-shelf sediments record history of twentieth-century retreat of Pine Island Glacier. *Nature*, *541*(7635), 77–80. doi: 10.1038/nature20136

Tsai, V. C., Stewart, A. L., & Thompson, A. F. (2015). Marine ice-sheet profiles and stability under Coulomb basal conditions. *Journal of Glaciology*, *61*(226), 205–215. doi: 10.3189/2015JoG14J221

van den Akker, T., Lipscomb, W., Leguy, G., Bernales, J., Berends, C., van de Berg, W. J., & van de Wal, R. S. W. (2023). Present-day mass loss rates are a precursor for West Antarctic Ice Sheet collapse. *Research Square*, *PREPRINT (*. Retrieved from `https://www.researchsquare.com/article/rs-3498111/v1` doi: https://doi.org/10.21203/rs.3.rs-3498111/v1

Walker, R. T., Parizek, B. R., Alley, R. B., Anandakrishnan, S., Riverman, K. L., & Christianson, K. (2013). Ice-shelf tidal flexure and subglacial pressure variations. *Earth and Planetary Science Letters*, *361*, 422–428. doi: 10.1016/j.epsl.2012.11.008

Weertman, J. (1974). Stability of the Junction of an Ice Sheet and an Ice Shelf. *Journal of Glaciology*, *13*(67), 3–11. doi: 10.1017/S0022143000023327

Wild, C. T., Alley, K. E., Muto, A., Truffer, M., Scambos, T. A., & Pettit, E. C. (2022). Weakening of the pinning point buttressing Thwaites Glacier, West Antarctica. *The Cryosphere*, *16*(2), 397–417. doi: 10.5194/tc-16-397-2022

Yu, H., Rignot, E., Seroussi, H., & Morlighem, M. (2018). Retreat of Thwaites Glacier, West Antarctica, over the next 100 years using various ice flow models, ice shelf melt scenarios and basal friction laws. *The Cryosphere*, *12*(12), 3861–3876. doi: 10.5194/tc-12-3861-2018

Zoet, L. K., & Iverson, N. R. (2020). A slip law for glaciers on deformable beds. *Science*, *368*(6486), 76–78. doi: 10.1126/science.aaz1183

Zwally, H. J., Giovinetoo, M. B., Beckley, M. A., & Saba, J. L. (2012). *Antarctic and Greenland Drainage Systems.* Retrieved 29-01-2024, from `https://earth.gsfc.nasa.gov/cryo/data/polar-altimetry/antarctic-and-greenland-drainage-systems`

Retreat of Thwaites Glacier Triggered by its Neighbours

Matt Trevers[1], Stephen L. Cornford[1], Antony J. Payne[2], Edward Gasson[3], Suzanne Bevan[4]

[1]Centre for Polar Observation and Modelling, School of Geographical Sciences, University of Bristol, Bristol, UK
[2]School of Environmental Sciences, University of Liverpool, Liverpool, UK
[3]Centre for Geography and Environmental Sciences, University of Exeter, Cornwall, UK
[4]Department of Geography, Faculty of Science and Engineering, Swansea University, Swansea, UK

Key Points:

- Limited retreat of present-day Thwaites Glacier in response to submarine melting of its floating ice shelf
- Dynamical interactions with its neighbours can drive very rapid and substantial retreat in Thwaites
- Extreme ice shelf forcing scenarios or reduced basal stress near the grounding line can also drive widespread grounding line retreat

Corresponding author: Matt Trevers, `matt.trevers@bristol.ac.uk`

Abstract

The Amundsen Sea Embayment in West Antarctica is experiencing the most rapid mass loss and grounding line retreat in Antarctica. Its glaciers are vulnerable to retreat through marine ice sheet instability. There is uncertainty over the timing and magnitude of retreat and in particular the response of Thwaites Glacier to thinning of its ice shelf and to ocean forced retreat of its neighbouring glaciers. We find that the response of Thwaites to melting of its ice shelf is limited. However, retreat of its neighbours can drive substantial retreat in Thwaites. We examine the impact of ice shelf buttressing on the stability of the grounding line. Further experiments show that extreme ice shelf forcings are required to trigger retreat in Thwaites in isolation. We also demonstrate that long-term stability is sensitive to the treatment of basal stress near the grounding line.

Plain Language Summary

Glaciers of the Amundsen Sea Embayment in West Antarctica, including Thwaites Glacier, are discharging ice to the oceans and contributing to rising sea levels faster than anywhere else in Antarctica. Thwaites' ice shelf, a floating extension of the glacier, is likely to disintegrate over coming decades. There is disagreement over the impact this will have on the flow of upstream ice, with some recent studies suggesting that the ice shelf is already so weakened that its loss will not have any major consequence. In line with those studies, we find that over millennial timescales Thwaites is not strongly affected by ocean-driven melting of its ice shelf, except in extreme ocean circulation scenarios. However we find that interactions with neighbouring glaciers can trigger widespread retreat across the Amundsen Sea Embayment through previously unexplored feedback processes. We also find that Thwaites' long-term stability is dependent on the physics of the ice-bed interface. Our results demonstrate that individual Antarctic glaciers cannot be modelled as isolated systems, and highlight the need for an improved understanding of basal conditions and processes.

1 Introduction

The largest uncertainty in projections of global sea level rise (SLR) over the coming centuries is due to the contribution of the Antarctic Ice Sheet (Church et al., 2013). The fastest present-day mass loss is occurring in the Amundsen Sea Embayment (ASE) in West Antarctica (Shepherd et al., 2018). Thinning rates of several meters per year are observed for the ice shelves and grounding regions of the ASE (B. E. Smith et al., 2020) driven by strong ocean warming and sub-shelf melting (e.g. Naughten et al., 2022; Holland et al., 2023). The ASE is at risk of rapid grounding line retreat by marine ice sheet instability (MISI; Weertman, 1974; Schoof, 2007), which could potentially lead to collapse of the marine-based sectors of the West Antarctic Ice Sheet (WAIS) (Hughes, 1981; Feldmann & Levermann, 2015a). MISI can occur when the grounding line is positioned on a retrograde bed slope below sea level. Buttressing arising from lateral drag in confined ice shelves or pinning on ice rises beneath unconfined tongues can confer stability to grounded ice on a retrograde bed slope (e.g. Dupont & Alley, 2005; Goldberg et al., 2009; Favier & Pattyn, 2015). Ocean-forced thinning of ice shelves therefore has the potential to trigger grounding line retreat (R. B. Alley et al., 2015).

The configuration of the ASE ice streams, shelves and drainage basins is shown in Figure 1. The Crosson/Dotson (CD) basin contains the complex system of (from west to east) Kohler, Smith, Pope and Haynes glaciers discharging ice into the confined Dotson and Crosson ice shelves which branch around Bear Peninsula. The CD shelves and their tributary glaciers have seen thinning, acceleration and grounding line retreat in recent years (Lilien et al., 2018), with retreat rates of up to 11.7 km/year observed for Pope Glacier in 2017 (Milillo et al., 2022). This retreat is hypothesised to be driven by strong ice-ocean interactions in newly opened cavities.

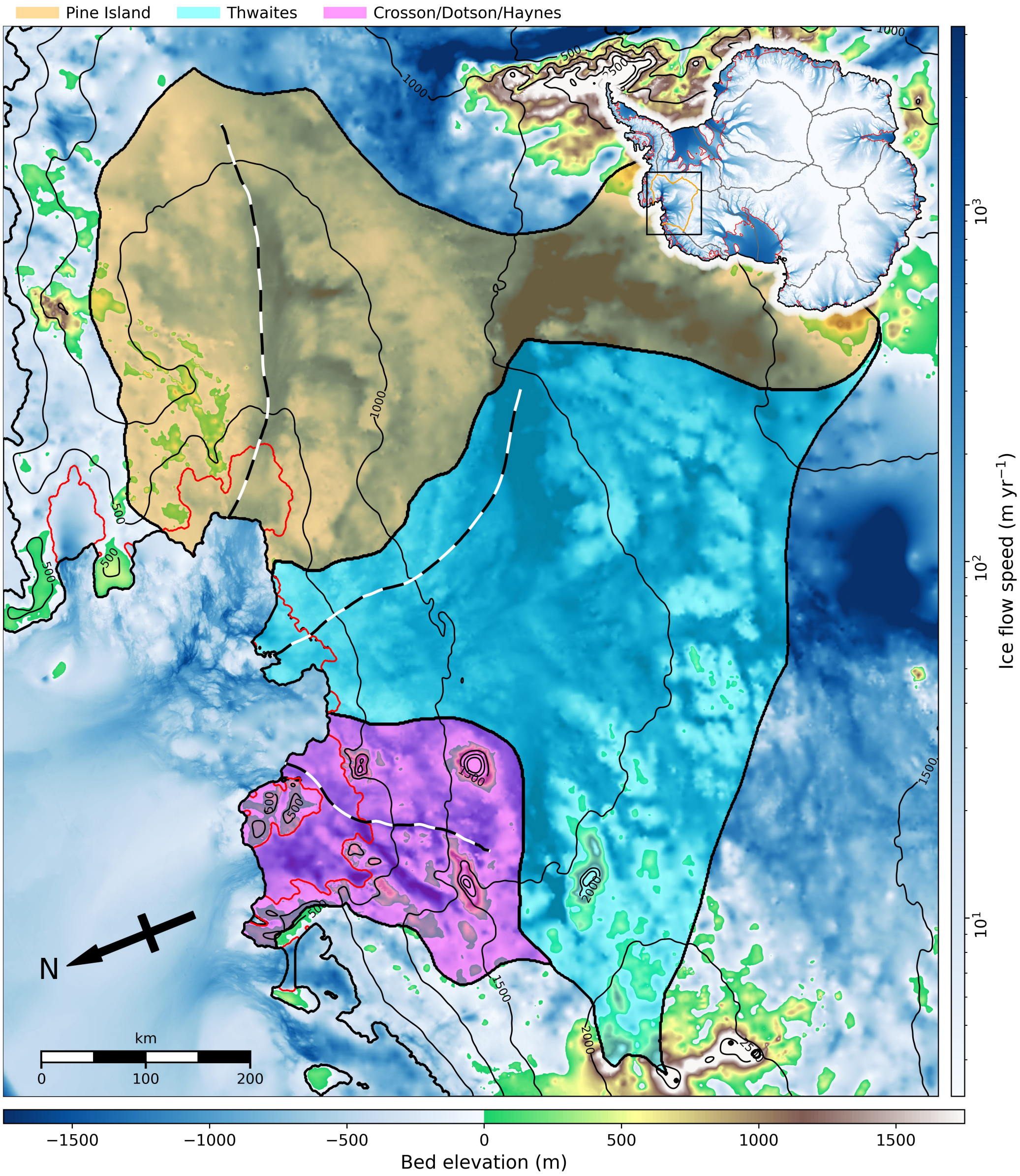

Figure 1. Bed topography of the ASE domain. Thick black lines show the initial ice front extent and basin boundaries, red lines the initial grounding line, thin black contours ice surface elevation and dashed black and white lines flowlines used in this study. Transparent shaded regions highlight individual glacier basins (Mouginot et al., 2017). The inset map shows Antarctic-wide flow speeds (Mouginot et al., 2019) with drainage boundaries from (Zwally et al., 2012). The black box shows the extent of the ASE domain within Antarctica.

Thwaites Glacier (TG) contains the sea level equivalent (SLE) of 0.6 m of ice and is one of the largest contributors to modern-day SLR (Holt et al., 2006). The grounding line retreated by 14 km from 1992 to 2011 (Rignot et al., 2014) and the mass loss rate increased by 22 Gt/year between 2006 and 2014 (Mouginot et al., 2014). The present-day grounding line is situated on a submarine ridge roughly 250 to 1000 m below sea level, with the bed rapidly deepening upstream. The TG ice shelf (TGIS) has undergone significant changes in recent decades (K. E. Alley et al., 2021). The TGIS is composed of the western ice tongue (TWIT) and the eastern ice shelf (TEIS) separated by a shear margin. TWIT detached from its pinning point around 2009 and rapidly disintegrated and accelerated (Miles et al., 2020). TEIS remains grounded on a pinning point near its ice front, confining TEIS and slowing ice flow relative to TWIT. TEIS initially accelerated following unpinning of TWIT but decelerated again as the shear margin weakened. The TEIS pinning point has progressively weakened due to thinning of TEIS since 2009 and may unpin entirely within a decade (Wild et al., 2022). Benn et al. (2022) suggested that backstress from the pinning point contributes to weakening and fracturing of TEIS as it thins.

Pine Island Glacier (PIG) is the single largest Antarctic contributor to SLR in recent decades (Rignot et al., 2019). It experienced significant 20th century retreat following ungrounding from a prominent seafloor ridge (J. A. Smith et al., 2017). Its present day grounding line is located in a constriction of the bed trough through which it discharges ice into its confined ice shelf (PIIS) (Reed et al., 2024). It has continued to thin and retreat in recent years (Mouginot et al., 2014; Rignot et al., 2019).

Both modelling and observational studies have suggested that MISI-driven retreat may already be underway for PIG and TG (e.g. Favier et al., 2014; Rignot et al., 2014; Mouginot et al., 2014; Joughin et al., 2014). More recent modelling studies have suggested a more limited SLR contribution by 2100, with the timing and magnitude of retreat sensitive to uncertain model parameters and the applied forcing (Yu et al., 2018; Alevropoulos-Borrill et al., 2020). Nias et al. (2016) found that unpinning of TEIS had negligible effect on the flow of grounded ice, while Benn et al. (2022) and Gudmundsson et al. (2023) both suggested that TEIS has limited buttressing impact and that its loss would be unlikely to trigger significantly increased ice discharge from TG.

A number of studies have demonstrated that dynamical interactions between neighbouring basins can significantly effect projected mass loss rates (Feldmann & Levermann, 2015a, 2015b; Martin et al., 2019). However ice sheet models commonly model isolated basins to limit the computational cost (e.g. Favier et al., 2014; Joughin et al., 2014; Seroussi et al., 2017) or whole ice sheets at reduced resolution (e.g. Feldmann & Levermann, 2015a; Golledge et al., 2015; DeConto et al., 2021). In this study we examine interbasin interactions within the ASE and their dynamical impact on the evolution of the individual basins over millennial timescales. We find that TG retreat can be driven by the evolution of its neighbours and we explore the mechanisms driving the interactions. We conduct an analysis of the buttressing strength for different configurations of the TG ice shelf and grounding line. Further experiments apply enhanced forcings to test the limits of TG's grounding line stability.

2 Methods

We used the BISICLES adaptive mesh refinement (AMR) ice flow model (Cornford et al., 2013). The AMR functionality enables mesh resolution of 500 m at the grounding line in concert with coarser resolution of 4 km for inland ice. A modern-day ASE initial condition comprising consistent fields of basal friction coefficient C, ice stiffening factor ϕ and a relaxed surface geometry was derived through an iterative procedure which follows Bevan et al. (2023); van den Akker et al. (2023) and which is detailed in Supporting Text S1. BedMachine v3 (Morlighem et al., 2020; Morlighem, 2022) provided bed topography and pre-initialisation ice geometry. Non-evolving surface accumulation rates came from the 1980 to 2021 mean of the MAR regional climate model (Agosta et al., 2019). The three dimensional temperature field was generated by a thermal spin-up which is described in Supporting Text S2. Model inputs are shown in Figure S3.

We carried out two sets of experiments, detailed separately below. The first set of experiments, described in Section 2.1, explore the dynamical interactions between drainage basins in the ASE. The second set, described in Section 2.2, apply a range of enhanced forcings to TG in isolation.

2.1 Interbasin Interactions

These experiments explored the response of the ASE to the focused regional application of basal melt, and the interactions between drainage basins. Sub-ice shelf melt was applied for 1000 years to the isolated PIG, TG and CD basins, the combinations of PIG+TG and CD+TG, and finally to all three basins combined. We applied the depth-dependent melt rate parameterisation described in Supporting Text S3 which reached a maximum of 250 m/year at a depth of 1000 m.

Basal stress for grounded ice was determined by a Regularised Coulomb friction law,

$$\boldsymbol{\tau}_{b,r} = -C\,|\boldsymbol{u}_b|^{m-1}\left(\frac{|\boldsymbol{u}_b|}{u_0}+1\right)^{-m}\cdot\boldsymbol{u}_b, \tag{1}$$

where C is the spatially varying friction coefficient, $\boldsymbol{u}_b$ the basal sliding velocity, $m = 1/3$ the friction law exponent and $u_0 = 50$ m/year the fast sliding speed. This expression is equivalent to that introduced by Joughin et al. (2019). A variable calving rate was applied at the ice front anti-parallel to the direction of ice flow,

$$\boldsymbol{u}_c = -r_c\cdot\boldsymbol{u}_T, \tag{2}$$

where $\boldsymbol{u}_T$ is the terminus velocity and r_c the constant calving multiplier. We set $r_c = 1$ to prohibit ice front advance, while retreat can still result from thinning.

Results and discussion of these experiments are presented in Section 3.1, along with an analysis of the buttressing strength for different configurations of the TG ice shelf and grounding line. Animated plots of all experiments in this section are provided with the supplementary material.

2.2 Thwaites Enhanced Forcings

In these experiments a range of enhanced forcings were applied to TG in order to probe the limits of stability of its grounding line. Experiments were continued from the final state after 1000 years of the TG melt experiment described in Section 2.1.

Sub-ice shelf melt was applied for a further 1000 years to the TG basin. Four sets of enhanced forcings were applied: (1) The depth-dependent melt rate described in Supporting Text S3 with a range of maximum values up to 2000 m/year at 1000 m depth. (2) Melting was applied uniformly across the ice shelf independent of depth, with a range of melt rates up to 1250 m/year. (3) Enhanced calving via a range of additional calving multipliers applied to floating ice in the TG basin with a draft of less than 100 m. (4) Application of an alternative Coulomb-limited friction law introduced by Tsai et al. (2015),

$$\boldsymbol{\tau}_{b,T} = -\frac{\boldsymbol{u}_b}{|\boldsymbol{u}_b|}\cdot\min\left[|\boldsymbol{\tau}_{b,r}|\,,\alpha N\right], \tag{3}$$

where $\alpha = 0.5$ is a dimensionless coefficient and N is the basal effective pressure. $\boldsymbol{\tau}_{b,r}$ was calculated from Equation 1. This expression, referred to as the Tsai law from hereon in, prohibits the basal stress from exceeding the effective pressure.

For all enhanced forcing experiments, model parameters from Section 2.1 were applied unless otherwise specified. Results and discussion of the response of TG to these enhanced forcings are presented in Section 3.2.

3 Results and Discussion

3.1 Interbasin Interactions

Figure 2 shows a contrast in the response of PIG and TG to melting of their ice shelves. Melting of PIIS lead to almost complete deglaciation of the marine-based parts of PIG within 1000 years, and complete or ongoing deglaciation of TG. PIG retreated in every experiment in which it was subjected to the melt forcing (dashed lines, Panel f). It retreated earlier than TG and at an almost identical rate between experiments, indicating that its retreat is unaffected by its neighbour. By contrast, TG did not retreat significantly when TGIS was melted in isolation (orange lines), with its grounding line restabilising a few tens of kilometers upstream of its initial position. Instead retreat of PIG was necessary to trigger more substantial retreat in TG. The retreat and thinning of PIG drove significant drawdown of ice from TG, seen as a large ice flux across the basin boundary (blue line, Panel g). This enhanced thinning of inland ice in TG drove retreat of its grounding line, which accelerated once it had retreated over deeper bed. Applying melt simultaneously to both basins (cyan lines) triggered earlier retreat in TG due to thinning from the combination of sources. The resulting simultaneous retreat in both basins lead to ice fluxes in alternating directions across the dividing boundary at different times (Panel g). At 525 years ASE mass loss peaked at $\sim$7 mm/year SLE, an order of magnitude faster than the current observed mass loss rate for the entire ice sheet (B. E. Smith et al., 2020). Grounding line retreat rates in TG peaked at $\sim$7 km/year which is within the observed range of retreat rates Milillo et al. (2022). Applying melt in all ASE basins (red lines) produced very similar patterns of mass loss, with retreat in TG triggered 50 years earlier.

Figure 3 shows the interactions between the CD and TG basins. With melt applied in isolation CD saw limited retreat, with its grounding line eventually restabilising in a retreated position up to $\sim$100 km upstream. Thinning in CD drove drawdown from TG across the dividing boundary (blue line, Panel g), but the associated thinning in TG wasn't sufficient to trigger retreat there. With melt was also applied to TG, the boundary ice flux into CD was initially smaller since TG was also thinning (cyan line, Panel g). The reduced inflow from TG drove further retreat in CD (Panel b), in turn driving increased inflow from TG after 325 years. The enhanced thinning of TG eventually lead to very rapid retreat of the TG grounding line (Panel f) and widespread deglaciation in both basins (Panels c, d).

Martin et al. (2019) demonstrated the importance of ice-dynamical interactions between basins at the regional scale. They found a modest increase in the rate of mass loss after $\sim$100 years when ASE melting was combined with melting in either the Eastern Ross Sector (including the Siple Coast ice streams) or the Western Ronne sector, as compared with the summed mass loss when melt was applied separately. Similarly, Feldmann and Levermann (2015a) showed that thinning and retreat in the ASE could cause migration of the upstream ice divide into the Ross and Filcher-Ronne drainage basins, ultimately triggering collapse in those basins after several thousand years. By contrast, interbasin interactions in our experiments drove significantly increased discharge within a few hundred years and could trigger collapse of the CD and TG basins within a thousand years. The interacting basins in our experiments are side-by-side neighbours with ice flowing parallel to dividing boundaries, thus flow reorganization can occur rapidly after the onset of retreat. In the earlier studies interactions occurred across the upstream ice divide, hence with a significant lag following the onset of ocean-driven thinning.

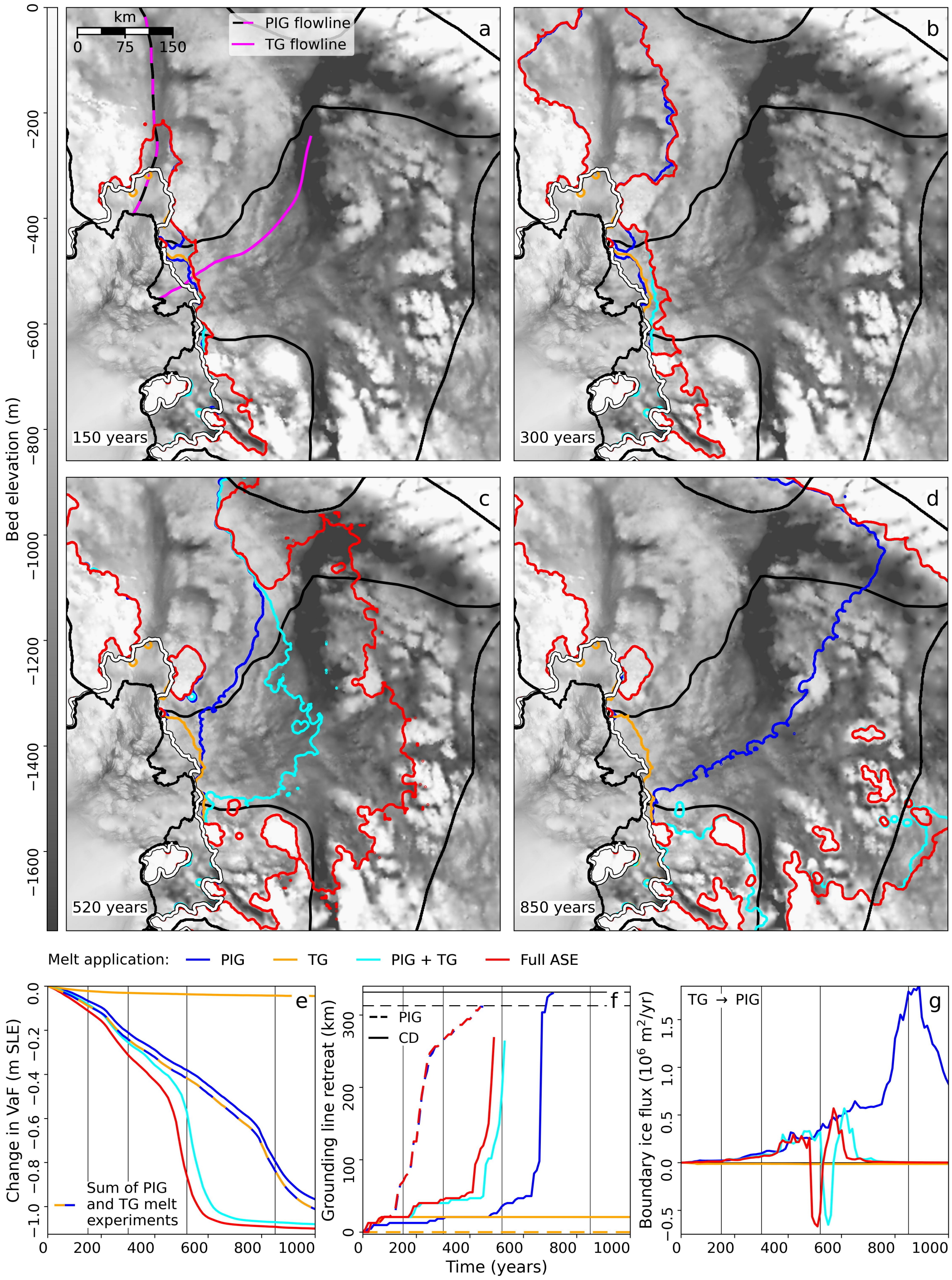

Figure 2. Maps and timeseries of the ASE evolution for PIG, TG, combined PIG+TG and full ASE melt experiments. (a) to (d) Grounding lines for all experiments (coloured lines) at selected snapshots. Also shown are the basin boundaries and initial ice front (black lines) and initial grounding lines (white lines with black edges). Panel (a) also shows PIG and TG flowlines. (e) Change in ASE Volume above Flotation (VaF), including the summed VaF change of the individual PIG and TG melt experiments. (f) Grounding line retreat in PIG (dashed lines) and TG (solid lines). Lines are truncated where the grounding line retreats beyond the end of the flowline. Black horizontal lines show the flowline extents in PIG and TG respectively. Note that blue, cyan and red dashed lines overlap. (g) Ice thickness flux per unit length across the PIG-TG basin boundary, defined such that positive flux refers to flow out of the TG basin. Vertical black lines in (e) to (g) refer to panels (a) to (d).

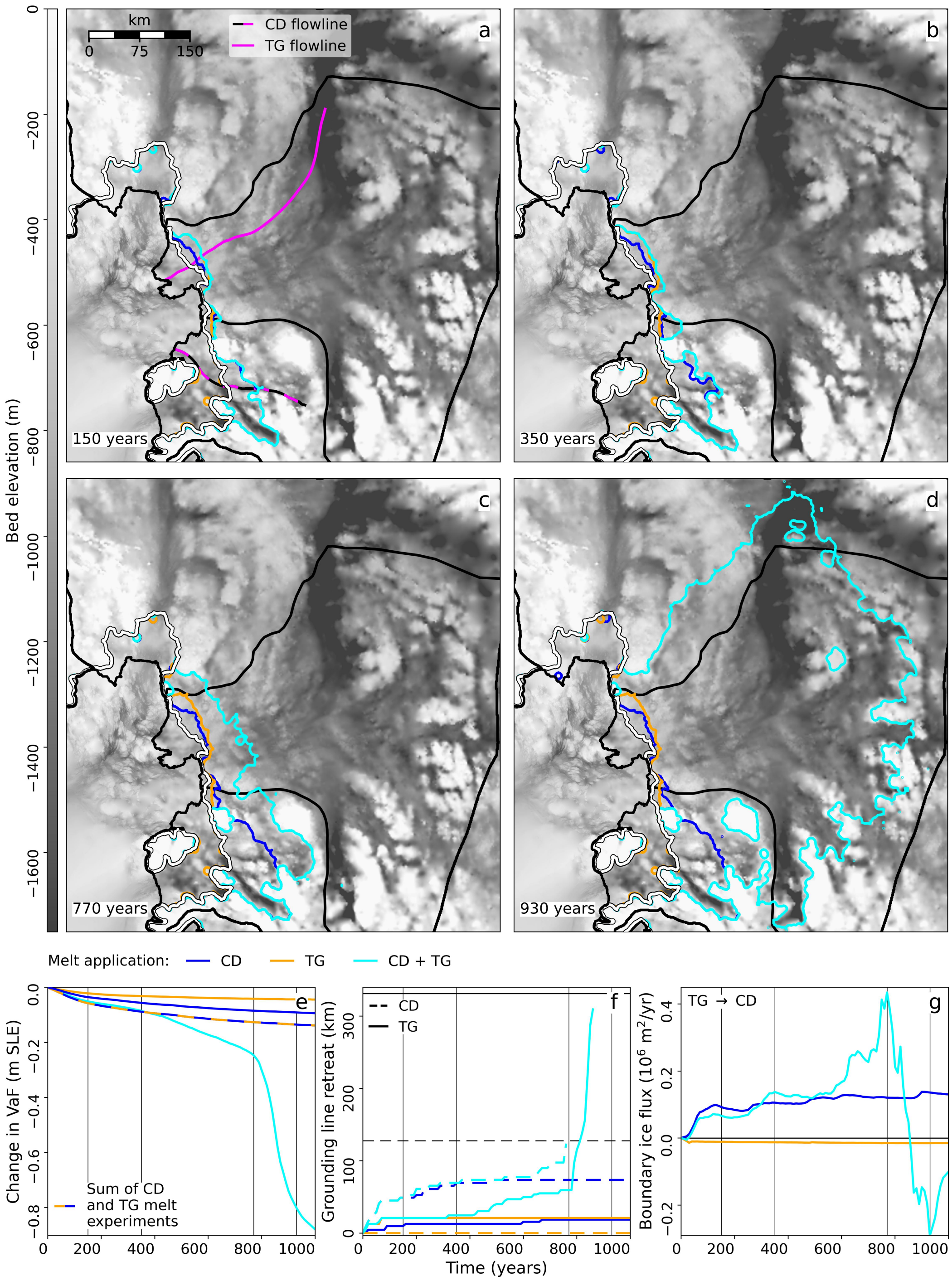

Figure 3. Maps and timeseries plots of the evolution of the ASE for CD, TG and combined CD+TG melt experiments. (a) to (g) as for Figure 2, except that the dashed blue and orange line in (e) shows the summed VaF loss from individual CD and TG melt experiments, dashed lines in (f) refer to the CD basin and fluxes in (g) are measured across the CD-TG basin boundary.

Gudmundsson et al. (2023) conducted an analysis of the strength of ice shelf buttressing in the ASE. They showed that TGIS provides limited buttressing compared with the PIG and CD shelves, and that much of the buttressing provided by TGIS could be explained by the small-scale embayments in the grounding line. We conduct a similar analysis by computing the buttressing number θ_n, the ratio of the resistive stress across the grounding line to the resistive stress in the absence of an ice shelf. The formulation of the buttressing number is described in Supporting Text S4. By definition $\theta_n = 1$ where there is zero buttressing. The ice shelf provides buttressing where $\theta_n < 1$, *anti-buttressing* where $\theta_n > 1$ and *super-buttressing* where $\theta_n < 0$. Figure S4 shows buttressing numbers calculated for TG grounding lines at the start and end of the isolated TG melt experiment (orange lines, Figure 2). Both configurations follow elevated features of the underlying bed. Local embayments were more heavily buttressed while convexities were often unbuttressed or even anti-buttressed. The histogram shows that the buttressing strength in the final configuration decreased relative to the initial state, indicating that grounding line stability was less dependent on the integrity of TGIS. Nonetheless, the final grounding line still contains some localised strongly buttressed regions which might be vulnerable to further degradation of TGIS. In three highlighted locations, the proximity of buttressed embayments in the final grounding line to overdeepened channels leading to the basin interior provide potential pathways to rapid retreat and deglaciation.

We studied the impact of unpinning TEIS by reducing the basal friction coefficient beneath the pinning point to zero in a diagnostic setting (Figure S5). This produced a significant instantaneous speedup for floating ice, but the speedup for grounded ice was limited to between 10 and 30% in a region within 25 km of the grounding line, focused on an anti-buttressed grounded protrusion. There was a minor reduction in the buttressing strength at the grounding line. A secondary pinning point located just downstream of the grounding line was found to have negligible impact on buttressing or the flow of TEIS. This demonstrates that while the pinning point constrains the flow of ice in TEIS, its buttressing effect on grounded ice is limited due to the highly fractured nature of TEIS. We find agreement with Benn et al. (2022) and Nias et al. (2016) who showed that unpinning of TEIS would have little impact on the discharge of grounded ice and is unlikely to immediately trigger marine ice sheet instability, although both studies used the same ice flow code as in this study. Wild et al. (2022) similarly found that ungrounding of TEIS produced only a 10% speedup across the grounding line.

3.2 Thwaites Enhanced Forcings

In Section 3.1 we showed that TG is not strongly sensitive to melting of its own ice shelf, with the grounding line restabilising a few tens of kilometers upstream. Additional thinning of upstream grounded ice driven by interactions with neighbouring glaciers was required to trigger more substantial retreat. The experiments in this section aim to establish whether TG is always resistant to standalone forcing.

Figure 4 shows the TG grounding line retreat in response to the enhanced forcings described in Section 2.2. These additional forcings were able to trigger substantial retreat in the TG basin, with more aggressive forcings producing earlier retreat. Retreat followed a similar pattern in all cases, with gradual retreat in short sporadic episodes until a final quasi-stable position was reached at 34 km. Further retreat from this position initiated rapid retreat as the bed deepens steeply upstream (Morlighem et al., 2020). The rate of retreat slowed again across a region between $\sim$75 and $\sim$125 km upstream before very rapid retreat was re-established, resulting in widespread deglaciation across the TG basin. Retreat rates peaked between 5 and 10 km/year during the most rapid phase of retreat (Figure S6). Figure S7 shows that the different types of forcing produced similar patterns of retreatt. Retreat tended to originate at the orange-highlighted embayment in Figure S4 and followed overdeepened channels cutting through the elevated bed region before reaching deeper bedrock further upstream. This demonstrates that de-

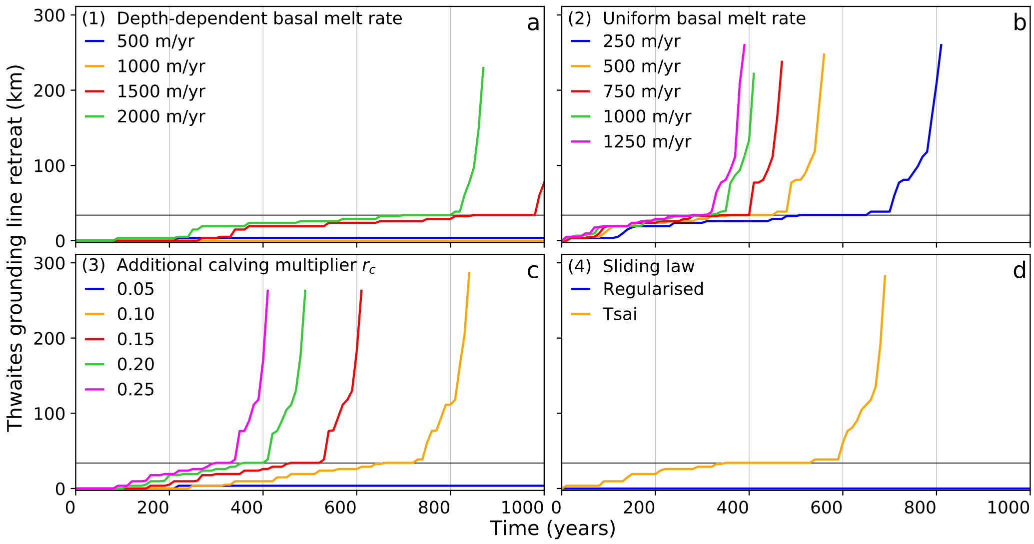

Figure 4. Grounding line retreat along the TG flowline for enhanced forcing experiments. Lines are truncated where the grounding line retreats beyond the end of the flowline, with the vertical scale covering the full flowline extent. Horizontal lines are drawn at 34 km.

spite TGIS being largely passive, localised remnant ice shelf embayments can still produce significant buttressing and their continued degradation can destabilise vulnerable portions of the grounding line. We stress that these enhanced melt rates are much higher than could be expected under modern conditions and are intended to establish the limits of stability.

A depth-dependent melt rate peaking at 1500 m/year at 1000 m depth (red line, Panel a) was required to trigger substantial retreat, whereas only 250 m/year of uniform melting (blue line, Figure 4b) triggered earlier retreat. The 1500 m/year depth-dependent melt forcing produced 572 Gt/year of melt across TGIS at the start of the experiment whereas the 250 m/year uniform melt forcing produced more melt at 684 Gt/year. The enhanced calving experiments (Panel c) produced similarly timed retreat to the uniform melt rates. The resulting calving rates which peak at 125 % of the shelf front velocity are seemingly within a realistic range (e.g. DeConto et al., 2021). However it should be noted that the calving rate forcing was designed to produce continual degradation of the ice shelf, and therefore unlike for the melt forcings it was impossible for the ice shelf to reach a balanced equilibrium with the calving rate.

Limiting the basal stress to the effective pressure with the application of the Tsai Law (Panel d, Equation 3) lowered the basal stress within a few kilometers upstream of the grounding line, triggering an instantaneous speedup of up to 500 m/year (Figure S8). This drove additional dynamic thinning, episodic grounding line retreat and further acceleration, eventually leading to rapid widespread retreat after 600 years. This sensitivity to the choice of sliding law reflects our uncertainty and lack of knowledge of basal condition, sliding mechanisms and grounding processes (e.g. Parizek et al., 2013; Joughin et al., 2019; Zoet & Iverson, 2020). Ice flow models commonly assume a discrete grounding line representing an abrupt transition from grounded ice upstream to floating ice downstream. In reality there is a less clearly defined grounding zone with variable grounding strength, driven by tidal motion (e.g. Ciracì et al., 2023). Walker et al. (2013) showed that tidal flexure of ice shelves could cause low tide uplift at centimeter scales a few kilometers upstream of the grounding line, with the possibility for seawater intrusions, while

Milillo et al. (2022) observed grounding zones up to 3 km in width for Pope, Smith and Kohler glaciers. Parizek et al. (2013) inferred the possibility of seawater influence up to 10 km inland from the grounding line. They showed that incorporating a grounding zone with decreased basal friction into a model of TG was able to trigger retreat. The reduction in basal stress generated by the Tsai law in our experiments occurred across similar distances upstream of the grounding line, creating an effective grounding zone. Our results therefore support their conclusions.

4 Conclusions

We have demonstrated that the dynamical interactions between neighbouring basins are a crucial component of the evolution of the ASE, and therefore important in assessing the stability of WAIS. TG was resistant to melting of TGIS in isolation, and required additional thinning generated by simultaneous melting of its neighbours to trigger substantial retreat. By contrast retreat of PIG was easily triggered and dominated the dynamics of its neighbours. We explored the limits of stability of TG and found that further degradation of TGIS through extreme melting or enhanced calving could tip the glacier into retreat. Our results provide further evidence that the present-day TGIS provides limited stability to the grounded glacier (e.g. Benn et al., 2022; Gudmundsson et al., 2023), but localised remnant ice shelf embayments can still produce sufficient buttressing to halt further retreat. An alternative sliding law mimicking a grounding zone with reduced ice-bed contact also produced rapid retreat after several centuries. Our study demonstrates that for projections beyond decadal timescales, individual glacier basins of WAIS cannot be considered as isolated systems. We also highlight the importance of improved model implementations of sliding processes and grounding zone conditions to inform more accurate projections of ice sheet evolution over coming centuries.

Open Research Section

The BISICLES ice sheet model is open source and is available for download from https://github.com/ggslc/bisicles-uob. The data on which this study is based are available in Mouginot et al. (2017), Agosta et al. (2019), Mouginot et al. (2019), Burton-Johnson et al. (2020), B. E. Smith et al. (2020) and Morlighem (2022). We did not generate any new observational data products.

Acknowledgments
The authors gratefully acknowledge helpful discussions with Paul Holland and Kaitlin Naughten. This research was carried out as part of the NSFGEO-NERC Pliocene sea level amplitudes (PLIOAMP) project (NE/T007397/1). MT was also partly funded by the UK NERC Centre for Polar Observation and Modelling (CPOM). This work used the ARCHER2 UK National Supercomputing Service (https://www.archer2.ac.uk) and the computational facilities of the Advanced Computing Research Centre, University of Bristol (http://www.bristol.ac.uk/acrc/).

References

Agosta, C., Amory, C., Kittel, C., Orsi, A., Favier, V., Gallée, H., ... Fettweis, X. (2019). Estimation of the Antarctic surface mass balance using the regional climate model MAR (1979–2015) and identification of dominant processes. *The Cryosphere*, *13*(1), 281–296. doi: 10.5194/tc-13-281-2019

Alevropoulos-Borrill, A. V., Nias, I. J., Payne, A. J., Golledge, N. R., & Bingham, R. J. (2020). Ocean-forced evolution of the Amundsen Sea catchment, West Antarctica, by 2100. *Cryosphere*, *14*(4), 1245–1258. doi: 10.5194/tc-14-1245-2020

Alley, K. E., Wild, C. T., Luckman, A., Scambos, T. A., Truffer, M., Pettit, E. C., … Dunmire, D. (2021). Two decades of dynamic change and progressive destabilization on the Thwaites Eastern Ice Shelf. *The Cryosphere*, *15*(11), 5187–5203. doi: 10.5194/tc-15-5187-2021

Alley, R. B., Anandakrishnan, S., Christianson, K., Horgan, H. J., Muto, A., Parizek, B. R., … Walker, R. T. (2015). Oceanic Forcing of Ice-Sheet Retreat: West Antarctica and More. *Annual Review of Earth and Planetary Sciences*, *43*(1), 207–231. doi: 10.1146/annurev-earth-060614-105344

Benn, D. I., Luckman, A., Åström, J. A., Crawford, A. J., Cornford, S. L., Bevan, S. L., … Bassis, J. (2022, jun). Rapid fragmentation of Thwaites Eastern Ice Shelf. *The Cryosphere*, *16*(6), 2545–2564. doi: 10.5194/tc-16-2545-2022

Bevan, S., Cornford, S. L., Gilbert, L., Otosaka, I., Martin, D., & Surawy-Stepney, T. (2023). Amundsen Sea Embayment ice-sheet mass-loss predictions to 2050 calibrated using observations of velocity and elevation change. *Journal of Glaciology*, 1–11. doi: 10.1017/jog.2023.57

Burton-Johnson, A., Dziadek, R., & Martin, C. (2020). Review article: Geothermal heat flow in Antarctica: current and future directions. *The Cryosphere*, *14*(11), 3843–3873. doi: 10.5194/tc-14-3843-2020

Church, J. A., Clark, P. U., Cazenave, A., Gregory, J. M., Jevrejeva, S., Levermann, A., … Unnikrishnan, A. A. (2013). Sea Level Change. In V. B. Stocker, T.F., D. Qin, G.-K. Plattner, M. Tignor, S.K. Allen, J. Boschung, A. Nauels, Y. Xia & P. Midgley (Eds.), *Climate change 2013: The physical science basis. contribution of working group i to the fifth assessment report of the intergovernmental panel on climate change* (pp. 1137–1216). Cambridge: Cambridge University Press. doi: 10.1017/CBO9781107415324.026

Ciracì, E., Rignot, E., Scheuchl, B., Tolpekin, V., Wollersheim, M., An, L., … Dini, L. (2023). Melt rates in the kilometer-size grounding zone of Petermann Glacier, Greenland, before and during a retreat. *Proceedings of the National Academy of Sciences*, *120*(20), 1–9. doi: 10.1073/pnas.2220924120

Cornford, S. L., Martin, D. F., Graves, D. T., Ranken, D. F., Le Brocq, A. M., Gladstone, R. M., … Lipscomb, W. H. (2013, jan). Adaptive mesh, finite volume modeling of marine ice sheets. *Journal of Computational Physics*, *232*(1), 529–549. doi: 10.1016/j.jcp.2012.08.037

DeConto, R. M., Pollard, D., Alley, R. B., Velicogna, I., Gasson, E., Gomez, N., … Dutton, A. (2021). The Paris Climate Agreement and future sea-level rise from Antarctica. *Nature*, *593*(7857), 83–89. doi: 10.1038/s41586-021-03427-0

Dupont, T. K., & Alley, R. B. (2005). Assessment of the importance of ice-shelf buttressing to ice-sheet flow. *Geophysical Research Letters*, *32*(4), 1–4. doi: 10.1029/2004GL022024

Favier, L., Durand, G., Cornford, S. L., Gudmundsson, G. H., Gagliardini, O., Gillet-Chaulet, F., … Le Brocq, A. M. (2014, feb). Retreat of Pine Island Glacier controlled by marine ice-sheet instability. *Nature Climate Change*, *4*(2), 117–121. doi: 10.1038/nclimate2094

Favier, L., & Pattyn, F. (2015, jun). Antarctic ice rise formation, evolution, and stability. *Geophysical Research Letters*, *42*(11), 4456–4463. doi: 10.1002/2015GL064195

Feldmann, J., & Levermann, A. (2015a). Collapse of the West Antarctic Ice Sheet after local destabilization of the Amundsen Basin. *Proceedings of the National Academy of Sciences*, *112*(46), 14191–14196. doi: 10.1073/pnas.1512482112

Feldmann, J., & Levermann, A. (2015b, apr). Interaction of marine ice-sheet instabilities in two drainage basins: simple scaling of geometry and transition time. *The Cryosphere*, *9*(2), 631–645. doi: 10.5194/tc-9-631-2015

Goldberg, D., Holland, D. M., & Schoof, C. (2009). Grounding line movement and ice shelf buttressing in marine ice sheets. *Journal of Geophysical Research: Earth Surface*, *114*(F4), 1–23. doi: 10.1029/2008JF001227

Golledge, N. R., Kowalewski, D. E., Naish, T. R., Levy, R. H., Fogwill, C. J., & Gasson, E. G. W. (2015). The multi-millennial Antarctic commitment to future sea-level rise. *Nature*, *526*(7573), 421–425. doi: 10.1038/nature15706

Gudmundsson, G. H., Barnes, J. M., Goldberg, D. N., & Morlighem, M. (2023). Limited Impact of Thwaites Ice Shelf on Future Ice Loss From Antarctica. *Geophysical Research Letters*, *50*(11), 1–11. doi: 10.1029/2023gl102880

Holland, P. R., Bevan, S. L., & Luckman, A. J. (2023). Strong Ocean Melting Feedback During the Recent Retreat of Thwaites Glacier. *Geophysical Research Letters*, *50*, 1–11. doi: 10.1029/2023GL103088

Holt, J. W., Blankenship, D. D., Morse, D. L., Young, D. A., Peters, M. E., Kempf, S. D., ... Corr, H. F. J. (2006, may). New boundary conditions for the West Antarctic Ice Sheet: Subglacial topography of the Thwaites and Smith glacier catchments. *Geophysical Research Letters*, *33*(9), 2–5. doi: 10.1029/2005GL025561

Hughes, T. J. (1981). The weak underbelly of the West Antarctic ice sheet. *Journal of Glaciology*, *27*(97), 518–525. doi: 10.3189/S002214300001159X

Joughin, I., Smith, B. E., & Medley, B. (2014). Marine Ice Sheet Collapse Potentially Under Way for the Thwaites Glacier Basin, West Antarctica. *Science*, *344*(6185), 735–738. doi: 10.1126/science.1249055

Joughin, I., Smith, B. E., & Schoof, C. (2019). Regularized Coulomb Friction Laws for Ice Sheet Sliding: Application to Pine Island Glacier, Antarctica. *Geophysical Research Letters*, *46*, 4764–4771. doi: 10.1029/2019GL082526

Lilien, D. A., Joughin, I., Smith, B. E., & Shean, D. E. (2018, apr). Changes in flow of Crosson and Dotson ice shelves, West Antarctica, in response to elevated melt. *The Cryosphere*, *12*(4), 1415–1431. doi: 10.5194/tc-12-1415-2018

Martin, D. F., Cornford, S. L., & Payne, A. J. (2019). Millennial-Scale Vulnerability of the Antarctic Ice Sheet to Regional Ice Shelf Collapse. *Geophysical Research Letters*, *46*(3), 1467–1475. doi: 10.1029/2018GL081229

Miles, B. W. J., Stokes, C. R., Jenkins, A., Jordan, J. R., Jamieson, S. S. R., & Gudmundsson, G. H. (2020). Intermittent structural weakening and acceleration of the Thwaites Glacier Tongue between 2000 and 2018. *Journal of Glaciology*, *66*(257), 485–495. doi: 10.1017/jog.2020.20

Milillo, P., Rignot, E., Rizzoli, P., Scheuchl, B., Mouginot, J., Bueso-Bello, J. L., ... Dini, L. (2022). Rapid glacier retreat rates observed in West Antarctica. *Nature Geoscience*, *15*(1), 48–53. doi: 10.1038/s41561-021-00877-z

Morlighem, M. (2022). *MEaSUREs BedMachine Antarctica, Version 3 [Data Set].* Retrieved 01-29-2024, from `https://nsidc.org/data/nsidc-0756/versions/3` doi: https://doi.org/10.5067/FPSU0V1MWUB6

Morlighem, M., Rignot, E., Binder, T., Blankenship, D., Drews, R., Eagles, G., ... Young, D. A. (2020). Deep glacial troughs and stabilizing ridges unveiled beneath the margins of the Antarctic ice sheet. *Nature Geoscience*, *13*(2), 132–137. doi: 10.1038/s41561-019-0510-8

Mouginot, J., Rignot, E., & Scheuchl, B. (2014). Sustained increase in ice discharge from the Amundsen Sea Embayment, West Antarctica, from 1973 to 2013. *Geophysical Research Letters*, *41*(5), 1576–1584. doi: 10.1002/2013GL059069

Mouginot, J., Rignot, E., & Scheuchl, B. (2019). *MEaSUREs Phase-Based Antarctica Ice Velocity Map, Version 1 [Data Set].* Retrieved 2024-01-29, from `https://nsidc.org/data/nsidc-0754/versions/1` doi: https://doi.org/10.5067/PZ3NJ5RXRH10

Mouginot, J., Scheuchl, B., & Rignot, E. (2017). *MEaSUREs Antarctic Boundaries for IPY 2007-2009 from Satellite Radar, Version 2 [Data Set].* Retrieved 2024-01-29, from `https://nsidc.org/data/nsidc-0709/versions/2` doi: https://doi.org/10.5067/AXE4121732AD

Naughten, K. A., Holland, P. R., Dutrieux, P., Kimura, S., Bett, D. T., & Jenkins, A. (2022). Simulated Twentieth-Century Ocean Warming in the

Amundsen Sea, West Antarctica. *Geophysical Research Letters*, *49*. doi: 10.1029/2021GL094566

Nias, I. J., Cornford, S. L., & Payne, A. J. (2016). Contrasting the modelled sensitivity of the Amundsen Sea Embayment ice streams. *Journal of Glaciology*, *62*, 552–562. doi: 10.1017/jog.2016.40

Parizek, B. R., Christianson, K., Anandakrishnan, S., Alley, R. B., Walker, R. T., Edwards, R. A., . . . Nowicki, S. M. J. (2013). Dynamic (in)stability of Thwaites Glacier, West Antarctica. *Journal of Geophysical Research: Earth Surface*, *118*(2), 638–655. doi: 10.1002/jgrf.20044

Reed, B., Green, J. A. M., Jenkins, A., & Gudmundsson, G. H. (2024). Recent irreversible retreat phase of Pine Island Glacier. *Nature Climate Change*, *14*(1), 75–81. doi: 10.1038/s41558-023-01887-y

Rignot, E., Mouginot, J., Morlighem, M., Seroussi, H., & Scheuchl, B. (2014). Widespread, rapid grounding line retreat of Pine Island, Thwaites, Smith, and Kohler glaciers, West Antarctica, from 1992 to 2011. *Geophysical Research Letters*, *41*(10), 3502–3509. doi: 10.1002/2014GL060140

Rignot, E., Mouginot, J., Scheuchl, B., van den Broeke, M., van Wessem, M. J., & Morlighem, M. (2019). Four decades of Antarctic Ice Sheet mass balance from 1979–2017. *Proceedings of the National Academy of Sciences*, *116*(4), 1095–1103. doi: 10.1073/pnas.1812883116

Schoof, C. (2007, sep). Ice sheet grounding line dynamics: Steady states, stability, and hysteresis. *Journal of Geophysical Research: Earth Surface*, *112*(F3), F03S28. doi: 10.1029/2006JF000664

Seroussi, H., Nakayama, Y., Larour, E., Menemenlis, D., Morlighem, M., Rignot, E., & Khazendar, A. (2017). Continued retreat of Thwaites Glacier, West Antarctica, controlled by bed topography and ocean circulation. *Geophysical Research Letters*, *44*(12), 6191–6199. doi: 10.1002/2017GL072910

Shepherd, A., Ivins, E., Rignot, E., Smith, B. E., van den Broeke, M. R., Velicogna, I., . . . Wouters, B. (2018). Mass balance of the Antarctic Ice Sheet from 1992 to 2017. *Nature*, *558*(7709), 219–222. doi: 10.1038/s41586-018-0179-y

Smith, B. E., Fricker, H. A., Gardner, A. S., Medley, B., Nilsson, J., Paolo, F. S., . . . Zwally, H. J. (2020). Pervasive ice sheet mass loss reflects competing ocean and atmosphere processes. *Science*, *368*(6496), 1239–1242. doi: 10.1126/science.aaz5845

Smith, J. A., Andersen, T. J., Shortt, M., Gaffney, A. M., Truffer, M., Stanton, T. P., . . . Vaughan, D. G. (2017). Sub-ice-shelf sediments record history of twentieth-century retreat of Pine Island Glacier. *Nature*, *541*(7635), 77–80. doi: 10.1038/nature20136

Tsai, V. C., Stewart, A. L., & Thompson, A. F. (2015). Marine ice-sheet profiles and stability under Coulomb basal conditions. *Journal of Glaciology*, *61*(226), 205–215. doi: 10.3189/2015JoG14J221

van den Akker, T., Lipscomb, W., Leguy, G., Bernales, J., Berends, C., van de Berg, W. J., & van de Wal, R. S. W. (2023). Present-day mass loss rates are a precursor for West Antarctic Ice Sheet collapse. *Research Square*, *PREPRINT (*. Retrieved from `https://www.researchsquare.com/article/rs-3498111/v1` doi: https://doi.org/10.21203/rs.3.rs-3498111/v1

Walker, R. T., Parizek, B. R., Alley, R. B., Anandakrishnan, S., Riverman, K. L., & Christianson, K. (2013). Ice-shelf tidal flexure and subglacial pressure variations. *Earth and Planetary Science Letters*, *361*, 422–428. doi: 10.1016/j.epsl.2012.11.008

Weertman, J. (1974). Stability of the Junction of an Ice Sheet and an Ice Shelf. *Journal of Glaciology*, *13*(67), 3–11. doi: 10.1017/S0022143000023327

Wild, C. T., Alley, K. E., Muto, A., Truffer, M., Scambos, T. A., & Pettit, E. C. (2022). Weakening of the pinning point buttressing Thwaites Glacier, West Antarctica. *The Cryosphere*, *16*(2), 397–417. doi: 10.5194/tc-16-397-2022

Yu, H., Rignot, E., Seroussi, H., & Morlighem, M. (2018). Retreat of Thwaites Glacier, West Antarctica, over the next 100 years using various ice flow models, ice shelf melt scenarios and basal friction laws. *The Cryosphere*, *12*(12), 3861–3876. doi: 10.5194/tc-12-3861-2018

Zoet, L. K., & Iverson, N. R. (2020). A slip law for glaciers on deformable beds. *Science*, *368*(6486), 76–78. doi: 10.1126/science.aaz1183

Zwally, H. J., Giovinetoo, M. B., Beckley, M. A., & Saba, J. L. (2012). *Antarctic and Greenland Drainage Systems.* Retrieved 29-01-2024, from `https://earth.gsfc.nasa.gov/cryo/data/polar-altimetry/antarctic-and-greenland-drainage-systems`

Supporting Information for "Retreat of Thwaites Glacier Triggered by its Neighbours"

Matt Trevers[1], Stephen L. Cornford[1], Antony J. Payne[2], Edward Gasson[3], Suzanne Bevan[4]

[1]Centre for Polar Observation and Modelling, School of Geographical Sciences, University of Bristol, Bristol, UK

[2]School of Environmental Sciences, University of Liverpool, Liverpool, UK

[3]Centre for Geography and Environmental Sciences, University of Exeter, Cornwall, UK

[4]Department of Geography, Faculty of Science and Engineering, Swansea University, Swansea, UK

Contents of this file

1. Text S1
2. Text S2
3. Text S3
4. Text S4
5. Figures S1 to S8

Additional Supporting Information (Files uploaded separately)

1. Information and Captions for Movies S1 to S8

Corresponding author: Matt Trevers, `matt.trevers@bristol.ac.uk`

S1. Model Initialisation

We initialised a modern-day configuration of the Amundsen Sea Embayment (ASE) to produce smooth and consistent fields of basal friction coefficient C, ice stiffening factor ϕ and a relaxed ice geometry. This was achieved through an iterative procedure following Bevan et al. (2023) which alternates model inversions to produce optimised fields of C and ϕ with relaxation cycles in which we allowed the surface geometry to evolve. We applied the most recently calculated fields of C and ϕ during each relaxation cycle, and the updated surface geometry was applied in the next iteration of the inverse problem. The initial ice thickness came from BedMachine v3 (Morlighem, 2022).

Fields of C and ϕ were estimated by solving an inverse problem. This method is described in detail in Cornford et al. (2013). In short, smooth fields of $C\left(x,y\right)$ and $\phi\left(x,y\right)$ are chosen that minimise the misfit between modelled and observed ice flow speeds. The observed flow speed came from (Mouginot et al., 2019). Where velocity observations are available we set as the initial guess at C,

$$C_0 = \frac{\phi_i g h \left|\nabla s\right|}{\left|\boldsymbol{u}_o\right| + 1}, \tag{S.1}$$

elsewhere and outside of the ASE basin boundary we set $C_0 = 10^5$. We initially set $\phi_0 = 1$. A nonlinear conjugate gradient method was applied to find a minimum of an objective function composed of the velocity misfit function and penalty functions for $C\left(x,y\right)$ and $\phi\left(x,y\right)$. The penalty functions act to limit the magnitude of spatial gradients of $C\left(x,y\right)$ and $\phi\left(x,y\right)$, with the Tikhonov coefficients determining the relative weightings of spatial gradients of $C\left(x,y\right)$ and $\phi\left(x,y\right)$ within the objective function. The inclusion of penalty functions in the objective function serves two purposes. Firstly, without it, the inverse problem would be under-determined, that is we would be seeking values of two unknown and unconstrained fields with only one field of input data. Secondly, it limits overfitting to small changes and noise in the observed velocity. Without the penalty functions the problem would be ill-conditioned.

During the relaxation cycle, we prohibited thinning or thickening for floating ice by calculating an additional basal mass balance which opposed any thickness change. Over grounded ice we applied the mean surface mass balance from 1980 to 2021 from the MAR regional climate model (Agosta et al., 2019), from which the observed rate of thickness change from Smith et al. (2020) was subtracted. This follows a method introduced by van den Akker et al. (2023) which is intended to optimise agreement with modern observed thickening/thinning rates in the final relaxed state once the observed thickness change rate component is removed from the applied surface mass balance.

The initialisation procedure was run for 50 years. The inverse problem was solved before the first timestep of the relaxation, and then again at 10 year intervals. During both the inversion and the relaxation cycles, a linear viscous sliding law was applied:

$$\boldsymbol{\tau}_{b,l} = -C_l \boldsymbol{u}_b. \tag{S.2}$$

The units and magnitude of C_l in Equation SS.2 differ from those of the Regularised law (Equation 1). Following the initialisation procedure, we therefore calculate C by equating $\boldsymbol{\tau}_{b,r} = \boldsymbol{\tau}_{b,l}$, taking the final modelled velocity at the end of the initialisation as $\boldsymbol{u}_b$.

Figure S1 shows the state at the end of the initialisation and Figure S2 shows the model state following 1 year of a forwards model run initialised from the relaxed model state. Figures S3e and S3f show the basal shear stress $\boldsymbol{\tau}_b$ (independent of sliding law) and ice stiffening factor ϕ produced by the initialisation procedure.

S2. Thermal Spin-up

The three dimensional temperature field used in this study was derived from a thermal spin-up using the BISICLES ice sheet model. The spin-up was carried out for the whole Antarctic Ice Sheet.

Initially an inverse problem was solved to generate a realistic velocity structure for the ice sheet using the observed velocities from (Mouginot et al., 2019). Note that unlike in Section S1, we simply performed a single model inversion rather than carrying out the full iterative procedure.

The spin-up was carried out for 100,000 years at a resolution of 8 km across the full ice sheet. The ice thickness was held constant throughout the spin-up. The ice column was divided into 24 vertical layers, with increasing vertical resolution towards the bed. The mean of monthly surface temperatures from 1980 to 2021 from the MAR regional climate model (Agosta et al., 2019) provided the surface temperature boundary condition. The mean geothermal heat flow dataset from Burton-Johnson et al. (2020) provided the basal boundary condition. This dataset was compiled as a mean of five products produced by different methods.

Following the spin-up, the temperature field for the ASE domain was extracted directly from the full Antarctic field. Figure S3d shows the depth averaged temperature field within the ASE.

S3. Ice Shelf Melt Rate

A synthetic ice shelf basal melt rate was applied in the experiments in this study. We used a very simple depth-dependent parameterisation in which the melt rate varied linearly from 1 m/year as sea level to some maximum melt rate at a depth of 1000 m, remaining constant with depth thereafter. i.e.,

$$\dot{m} = 1 + (\dot{m}_{max} - 1)\,\frac{\min\left[d, 1000\right]}{1000}, \tag{S.3}$$

where $\dot{m}$ is the melt rate (defined such that positive $\dot{m}$ means removal of ice) and d is the ice shelf draft. We maintain the 1 m/year melt rate at sea level to remove thin floating ice.

The interbasin interaction experiments described in Section 2.1 use $\dot{m}_{max} = 250$ m/year. This is sufficiently large to trigger retreat while also remaining within a plausible range for a future warming scenario. It initially produced 272 Gt/year total melt from TGIS and 569 Gt/year from PIIS. While the synthesised total melt was significantly higher than observed melt of up to 100 Gt/year for both PIIS and TGIS (Rignot et al., 2013; Shean et al., 2019), melt rates of up to 250 m/year near the grounding line are consistent with both ocean models and observations (Shean et al., 2019; Holland et al., 2023).

The first group of enhanced forcing experiments described in Section 2.2 also use this depth-dependent parameterisation, but taking different values of $\dot{m}_{max}$ up to 2000 m/year.

Melting was applied only to the underside of floating ice. Masks were used to selectively apply melt either individually to the PIG, TG or CD basins or to combinations of these basins. Basin extents were provided by Mouginot et al. (2017). Melting was confined to the selected basins even where grounding lines retreated beyond basin boundaries, and to cells with direct ocean connectivity.

S4. Buttressing Number Calculation

The strength of ice shelf buttressing can be evaluated using the buttressing number, θ_n. We follow the formulation of Gudmundsson et al. (2023) which we repeat here for convenience. The buttressing number is calculated as the ratio of the resistive horizontal stress measured normal to the grounding line to the resistive stress in the absence of an ice shelf,

$$\theta_n = \frac{R_n}{R_0}, \tag{S.4}$$

where R_n is the normal component of the resistive stress vector measured across the grounding line,

$$R_n = \hat{\boldsymbol{n}}_{nl}^T \cdot \boldsymbol{R}\hat{\boldsymbol{n}}_{nl}. \tag{S.5}$$

$\hat{\boldsymbol{n}}_{nl} = [n_x \;\; n_y]^T$ is the unit vector normal to the grounding line and $\boldsymbol{R}$ is the resistive stress vector,

$$\boldsymbol{R} = \begin{pmatrix} 2\tau_{xx} + \tau_{yy} & \tau_{xy} \\ \tau_{xy} & \tau_{xx} + 2\tau_{yy}, \end{pmatrix} \tag{S.6}$$

resulting in

$$R_n = n_x^2 \left(2\tau_{xx} + \tau_{yy}\right) + 2n_x n_y \tau_{xy} + n_y^2 \left(\tau_{xx} + 2\tau_{yy}\right). \tag{S.7}$$

R_0 is the normal component of the resisitive horizontal stress in the absence of an ice shelf,

$$R_0 = \frac{1}{2}\rho_i \left(1 - \rho_i/\rho_w\right) gh, \tag{S.8}$$

where $\rho_i = 917$ kg m^{-1} and $\rho_w = 1027$ kg m^{-1} are the ice and ocean densities respectively, $g = 9.81$ m s^{-2} is the gravitational acceleration and h is the ice thickness.

An unbuttressed or exposed grounding line will have $R_n = R_0$, therefore by definition $\theta_n = 1$. The ice shelf provides buttressing where $\theta_n < 1$, and *anti-buttressing* where $\theta_n > 1$, i.e. the presence of the shelf acts to increase tension at the grounding line. Where $\theta_n < 0$ the ice shelf provides *super-buttressing*, i.e. the buttressing strength is such that ice at the grounding line is under compression.

Figures S1 to S8

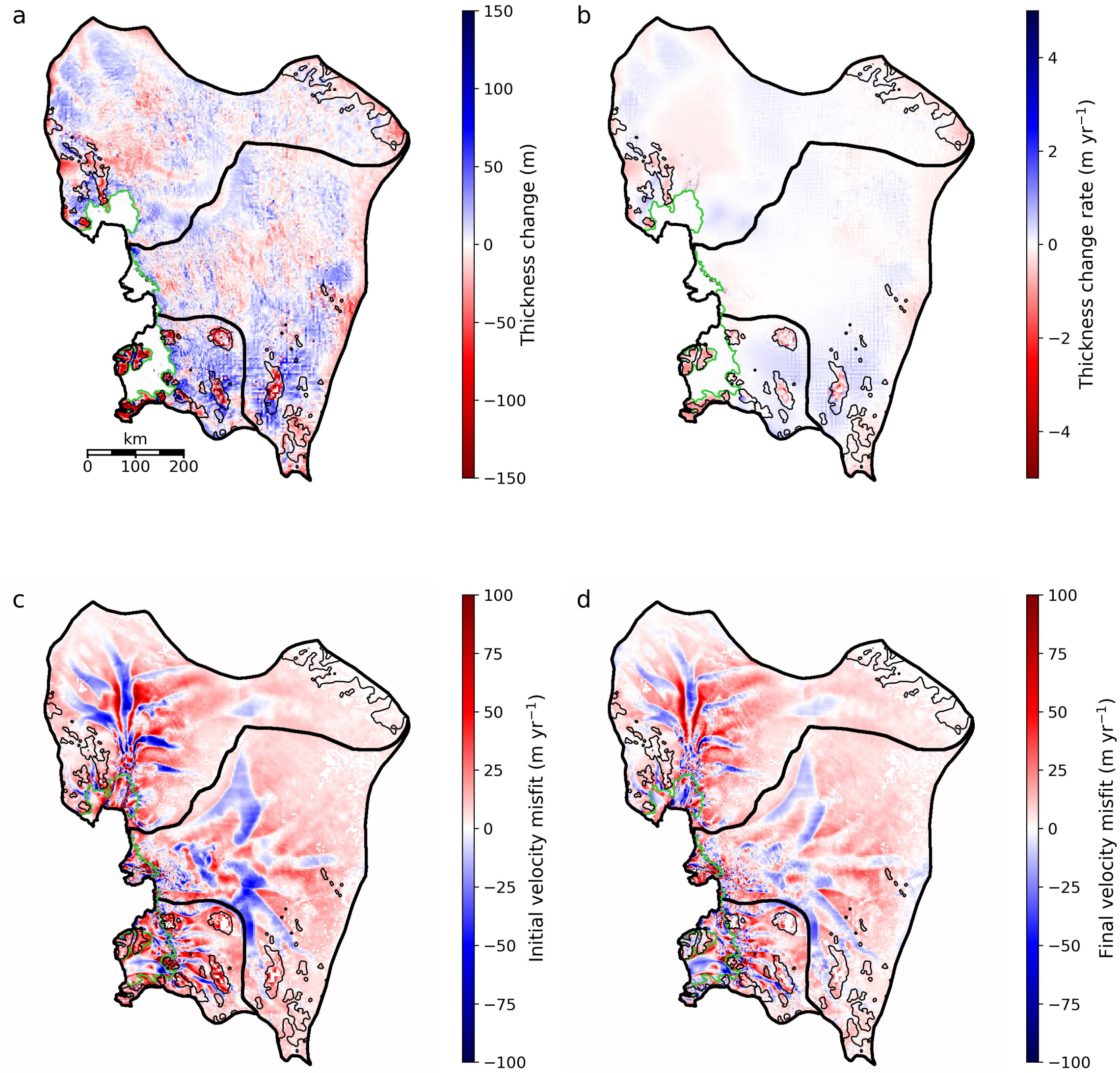

Figure S1. Initial state following the 50 year initialisation procedure. (a) Total thickness change from the original ice thickness. (b) Rate of thickness change after 50 years in the final relaxation iteration. (c) Initial ice velocity misfit. (d) Final ice velocity misfit. Thick black lines show the basin boundaries and ice extent while thin black lines show the sea level contour of bed depth. Grounding lines are marked by green lines.

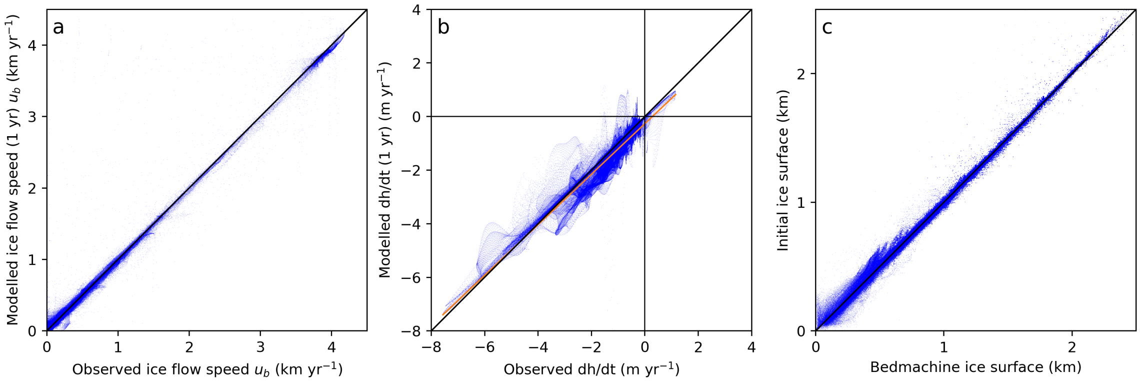

Figure S2. Model state following the first year of a forwards run started from the initial state shown in Figure S1. Scatterplots of: (a) Modelled versus observed ice flow speed. (b) Modelled versus observed rate of thickness change sampled where the flow speed exceeds 100 m/year, with orange line of best fit. (c) Initial ice surface elevation versus BedMachine v3 ice surface.

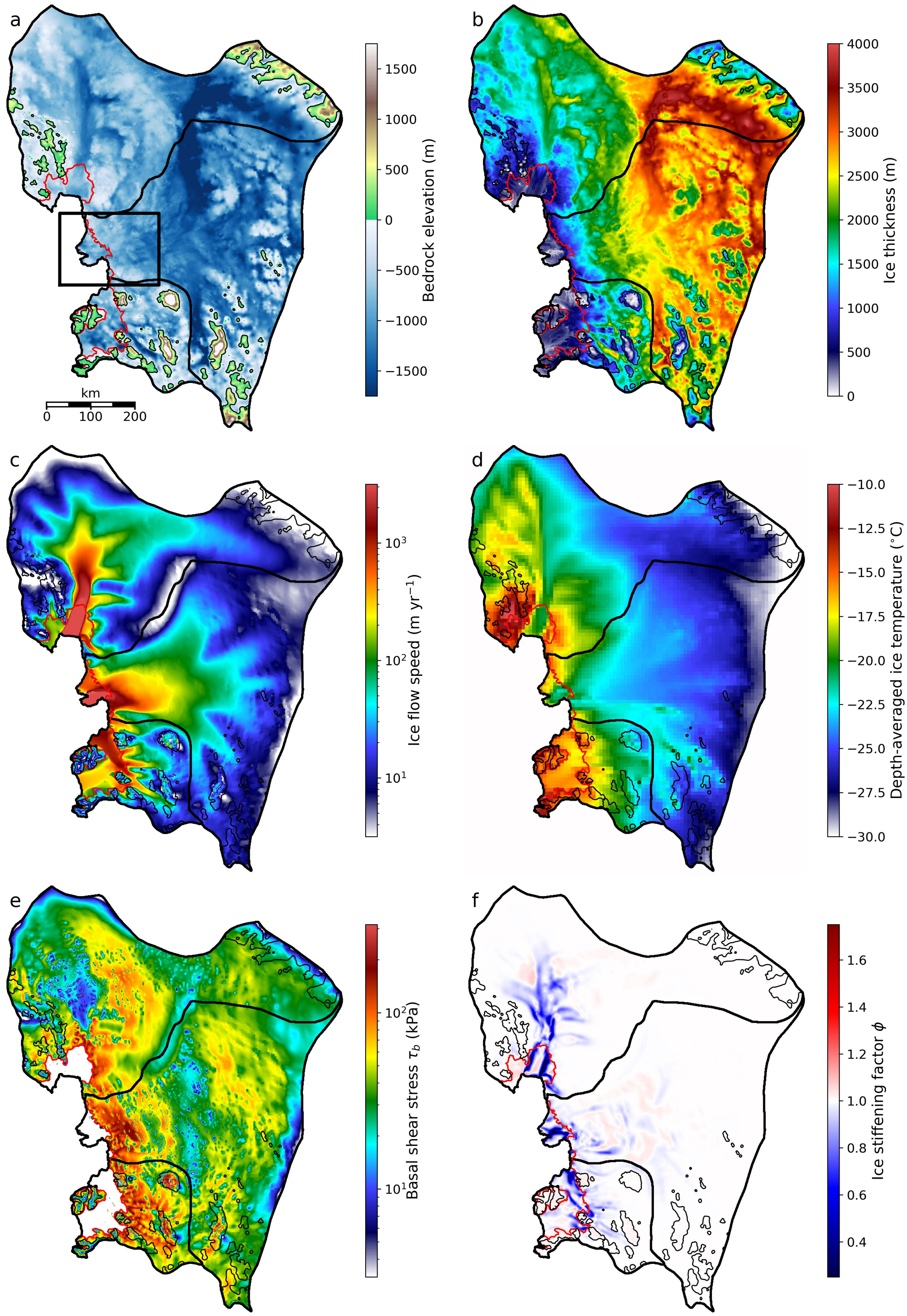

Figure S3. Model inputs following the initialization, shown only within the ASE. (a) Bed topography, (b) ice thickness, (c) modelled ice flow speed, (d) depth-averaged ice temperature, (e) basal shear stress and (f) ice stiffening factor. Thick black contours outline the drainage basins, thin black contours show the sea level contour of bed depth and red lines highlight the grounding line. The basal friction coefficient C is set to be large beyond the ASE boundary to effectively isolate the ASE. The box in (a) shows the spatial extent of other figures.

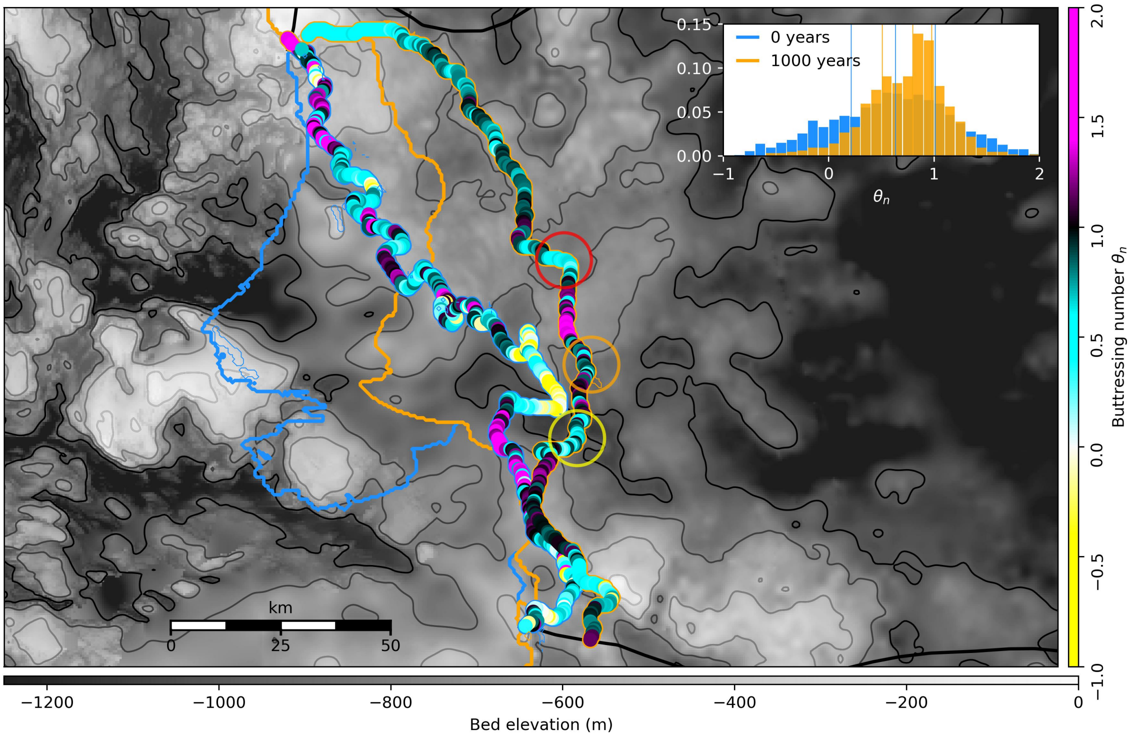

Figure S4. Buttressing numbers calculated for the TG grounding line for the initial and final states. Thick blue and orange lines mark the ice extent and thick black lines mark the TG basin boundary. Plotted buttressing factors are bordered in blue or orange to indicate the epoch. Coloured circles highlight potential vulnerabilities. The inset histogram shows grounding line buttressing numbers with quartile values highlighted by vertical lines. The extent of the zoomed in region is shown in Figure S3a. Bed contours at 250, 500, 750 and 1000 m depth are marked by grey/black contours of increasing darkness.

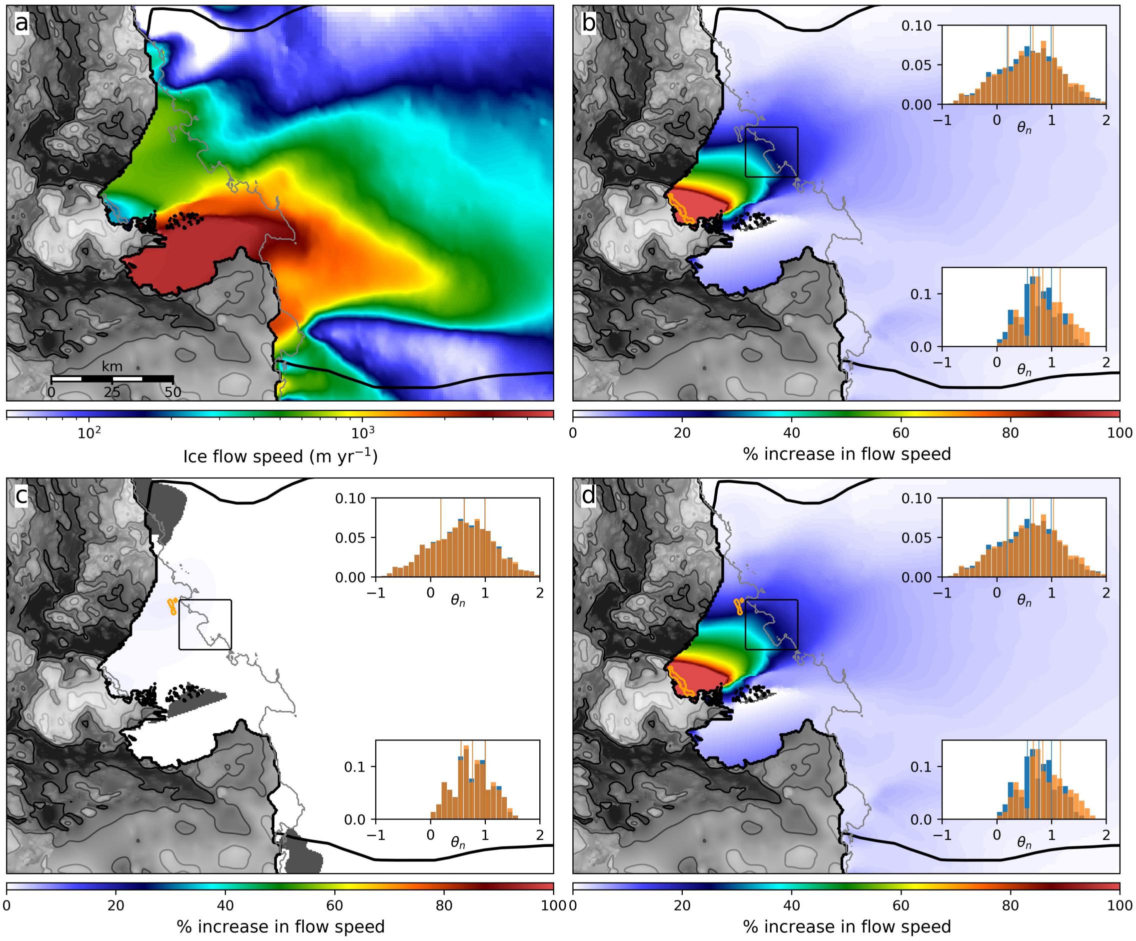

Figure S5. Impact of pinning point removal. (a) Ice flow speed for TG ice shelf and grounding line region. (b) to (d) Instantaneous percentage increase in flow speed associated with removal of the orange-highlighted pinning points. Pinning points were removed by setting the basal friction coefficient to those cells to zero. Regions that saw a slowdown are shown in grey. Inset histograms in (b) to (d) show the shift in buttressing number θ_n before (blue) and after (orange) pinning point removal. The upper histogram in each panel shows buttressing numbers calculated for all grounding lines cells (excluding pinning points) within the TG basin, while the lower histogram shows buttressing numbers calculated for the region within the black box. The extent of the zoomed in region is shown in Figure S3a. Bed maps and contours in each panel follow the same scale as in Figure S4.

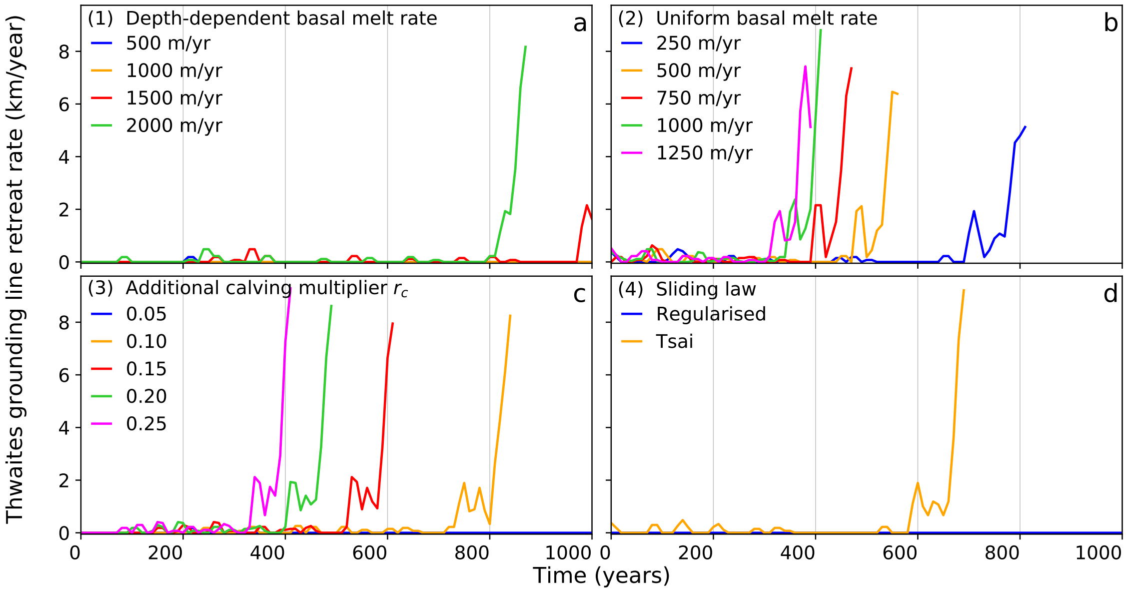

Figure S6. Grounding line retreat rates along the TG flowline for enhanced forcing experiments (see Figure 4).

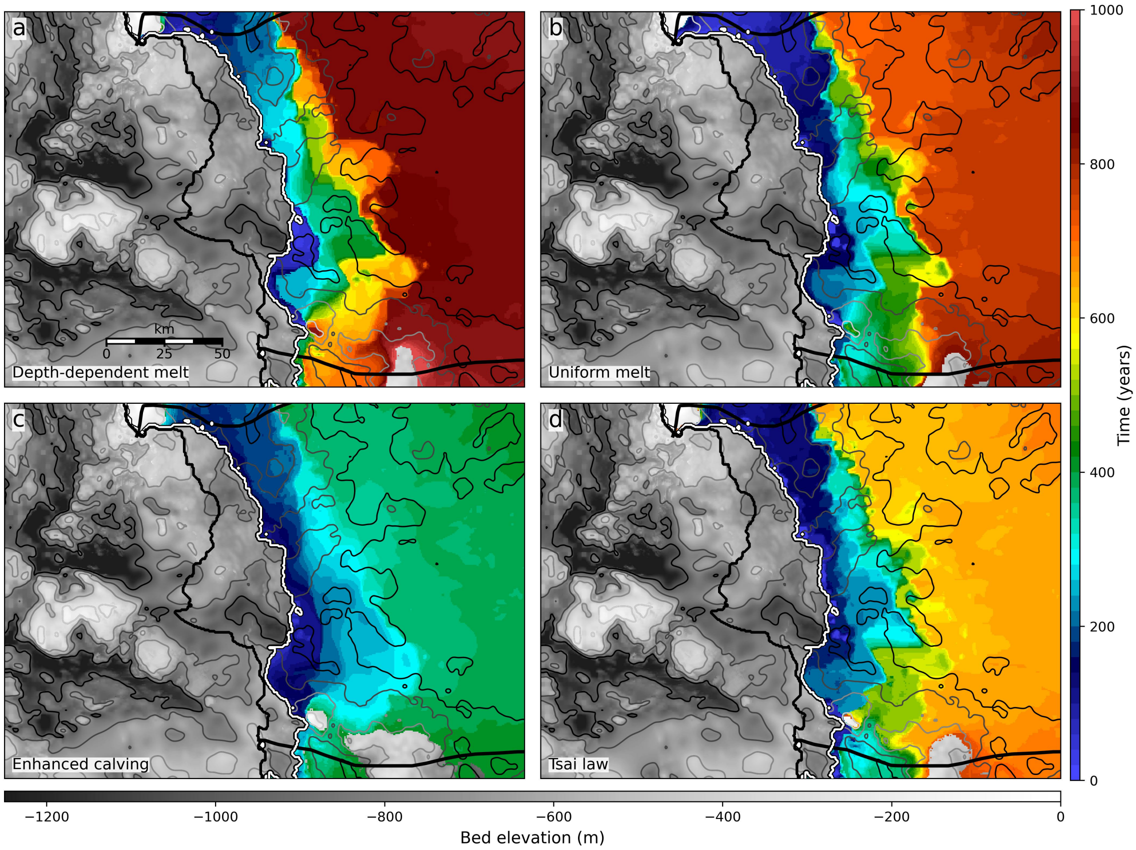

Figure S7. Time of earliest ungrounding in TG continuation experiments: (a) Depth-dependent melt rate 2000 m/yr. (b) Uniform melt rate 250 m/yr. (c) Additional calving rate with rate multiplier 1.25. (d) Tsai sliding law.The extent of the zoomed in region is shown in Figure S3a. Bed map and contours in each panel follow the same scale as in Figure S4.

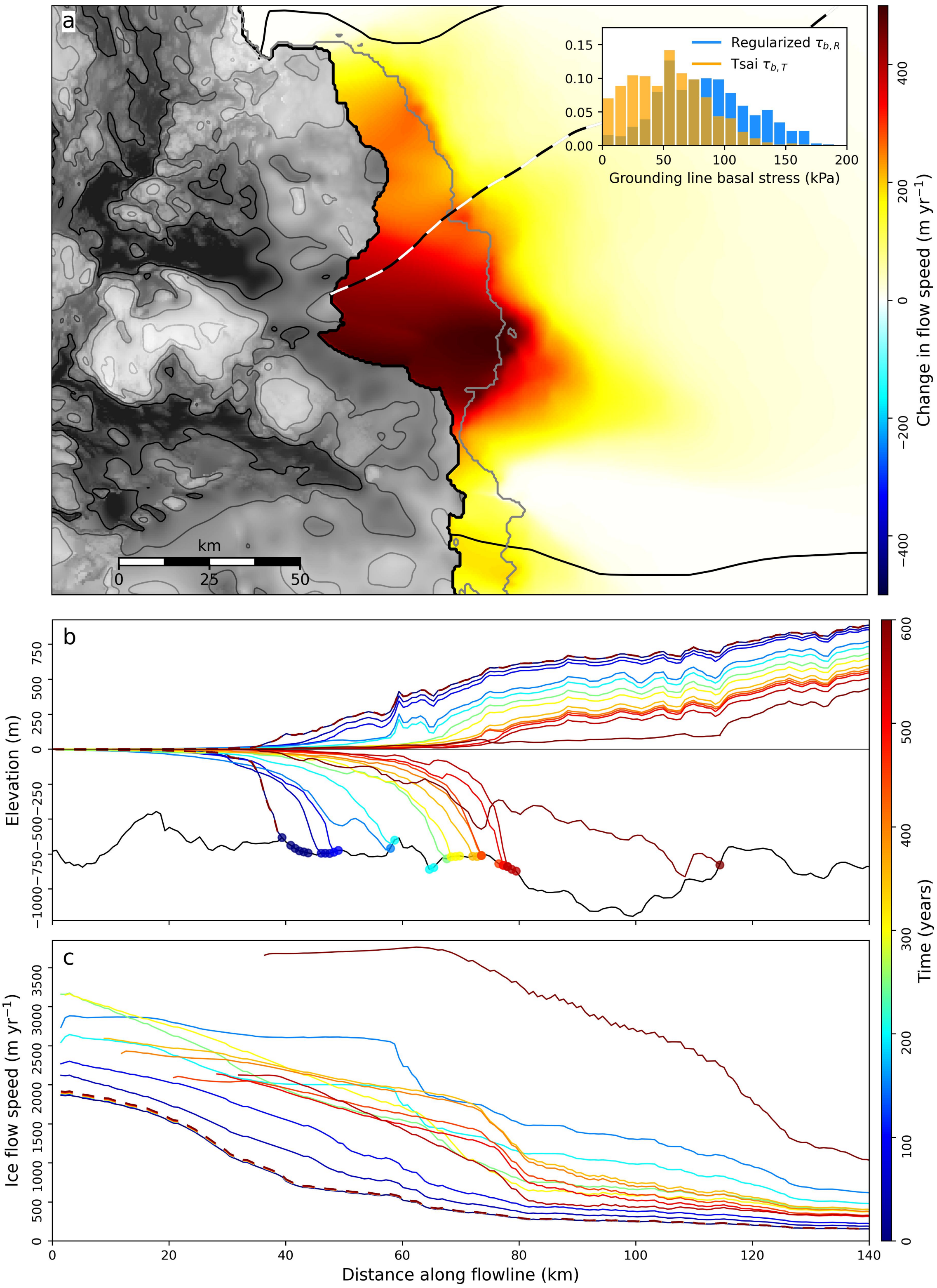

Figure S8. Comparison of Tsai and Regularised sliding law experiments (Figure 4d). (a) Instantaneous speedup when the Tsai law was applied. The inset histogram shows basal stress sampled at the grounding line for Regularised (blue) and Tsai (orange) laws. The extent of the zoomed in region is shown in Figure S3a. Bed map and contours in (a) follow the same scale as in Figure S4. (b) and (c) respectively show ice geometry and velocity along the flowline (black and white line, panel (a)) at 50-year intervals. Solid lines in (b) and (c) show the Tsai law while dashed lines show the Regularised law. Note that dashed lines overlap due to stagnation with the Regularised law. Circles plotted at the bed in (b) show where the Tsai rule determines the basal stress.

Information and Captions for Movies S1 to S8

We include animated plots of the experiments presented in Section 3.1. Movies S1 and S2 visualise the experiment groupings from Figures 2 and 3 respectively, while Movies S3 to S8 show individual experiments. Table S1 contains information on Movies S1 to S8.

Movie S1. Movie visualisation of Figure 2, showing the evolution of the ASE for PIG, TG, combined PIG and TG and full ASE melt experiments. (a) Grounding line evolution (coloured lines). Also shown are the basin boundaries and initial ice front (black lines) and initial grounding line (white lines with black edges) superimposed over the bed topography. The PIG and TG flowlines are also shown. (b) Volume above flotation (VaF) loss from the ASE. The dashed blue and orange line shows the summed VaF loss from the individual PIG and TG melt experiments. (c) Grounding line retreat along flowlines in PIG (dashed lines) and TG (solid lines). Lines are truncated where the grounding line retreats beyond the end of the flowline, shown by black horizontal lines. (d) Ice flux per unit length across the PIG-TG basin boundary, defined such that positive flux refers to flow out of the TG basin. (b) to (d) also include timesliders referencing the current time in (a).

Movie S2. Movie visualisation of Figure 3, showing the evolution of the ASE for CD, TG and combined CD and TG melt experiments. (a) to (d) as for Movie S1, except that dashed lines in (c) refer to the CD basin and fluxes in (d) are measured across the CD-TG basin boundary.

Movies S3 to S8. Movie visualisations of individual experiments. (a) to (d) as for Movies S1 and S2, except that (a) additionally shows the total thickness change. Dashed lines in (c) and fluxes in (d) refer to different basins depending on the experiment. See Table S1 for these details.

Movie	**Experiments**	**Retreat flowline**	**Basin boundary**	**Corresponding figure**
S1	PIG isolated melt TG isolated melt Combined PIG+TG melt Full ASE melt (CD+PIG+TG)	PIG	PIG-TG	Figure 2
S2	CD isolated melt TG isolated melt Combined CD+TG melt	CD	CD-TG	Figure 3
S3	PIG isolated melt	PIG	PIG-TG	Figure 2
S4	TG isolated melt	PIG	PIG-TG	Figure 2
S5	Combined PIG+TG melt	PIG	PIG-TG	Figure 2
S6	Full ASE melt (CD+PIG+TG)	PIG	PIG-TG	Figure 2
S7	CD isolated melt	CD	CD-TG	Figure 3
S8	Combined CD+TG melt	CD	CD-TG	Figure 3

Table S1. Details of Movies S1 to S8. Retreat flowlines refer to dashed lines in Panel c. Basin boundaries refer to Panel d.

References

Agosta, C., Amory, C., Kittel, C., Orsi, A., Favier, V., Gallée, H., ... Fettweis, X. (2019). Estimation of the Antarctic surface mass balance using the regional climate model MAR (1979–2015) and identification of dominant processes. *The Cryosphere*, *13*(1), 281–296. doi: 10.5194/tc-13-281-2019

Bevan, S., Cornford, S. L., Gilbert, L., Otosaka, I., Martin, D., & Surawy-Stepney, T. (2023). Amundsen Sea Embayment ice-sheet mass-loss predictions to 2050 calibrated using observations of velocity and elevation change. *Journal of Glaciology*, 1–11. doi: 10.1017/jog.2023.57

Burton-Johnson, A., Dziadek, R., & Martin, C. (2020). Review article: Geothermal heat flow in Antarctica: current and future directions. *The Cryosphere*, *14*(11), 3843–3873. doi: 10.5194/tc-14-3843-2020

Cornford, S. L., Martin, D. F., Graves, D. T., Ranken, D. F., Le Brocq, A. M., Gladstone, R. M., ... Lipscomb, W. H. (2013, jan). Adaptive mesh, finite volume modeling of marine ice sheets. *Journal of Computational Physics*, *232*(1), 529–549. doi: 10.1016/j.jcp.2012.08.037

Gudmundsson, G. H., Barnes, J. M., Goldberg, D. N., & Morlighem, M. (2023). Limited Impact of Thwaites Ice Shelf on Future Ice Loss From Antarctica. *Geophysical Research Letters*, *50*(11), 1–11. doi: 10.1029/2023gl102880

Holland, P. R., Bevan, S. L., & Luckman, A. J. (2023). Strong Ocean Melting Feedback During the Recent Retreat of Thwaites Glacier. *Geophysical Research Letters*, *50*, 1–11. doi: 10.1029/2023GL103088

Morlighem, M. (2022). *MEaSUREs BedMachine Antarctica, Version 3 [Data Set].* Retrieved 01-29-2024, from `https://nsidc.org/data/nsidc-0756/versions/3` doi: https://doi.org/10.5067/FPSU0V1MWUB6

Mouginot, J., Rignot, E., & Scheuchl, B. (2019). *MEaSUREs Phase-Based Antarctica Ice Velocity Map, Version 1 [Data Set].* Retrieved 2024-01-29, from `https://nsidc.org/data/nsidc-0754/versions/1` doi: https://doi.org/10.5067/PZ3NJ5RXRH10

Mouginot, J., Scheuchl, B., & Rignot, E. (2017). *MEaSUREs Antarctic Boundaries for IPY 2007-2009 from Satellite Radar, Version 2 [Data Set].* Retrieved 2024-01-29, from `https://nsidc.org/data/nsidc-0709/versions/2` doi: https://doi.org/10.5067/AXE4121732AD

Rignot, E., Jacobs, S., Mouginot, J., & Scheuchl, B. (2013, jul). Ice-Shelf Melting Around Antarctica. *Science*, *341*(6143), 266–270. doi: 10.1126/science.1235798

Shean, D. E., Joughin, I. R., Dutrieux, P., Smith, B. E., & Berthier, E. (2019). Ice shelf basal melt rates from a high-resolution digital elevation model (DEM) record for Pine Island Glacier, Antarctica. *The Cryosphere*, *13*(10), 2633–2656. doi: 10.5194/tc-13-2633-2019

Smith, B. E., Fricker, H. A., Gardner, A. S., Medley, B., Nilsson, J., Paolo, F. S., ... Zwally, H. J. (2020). Pervasive ice sheet mass loss reflects competing ocean and atmosphere processes. *Science*, *368*(6496), 1239–1242. doi: 10.1126/science.aaz5845

van den Akker, T., Lipscomb, W., Leguy, G., Bernales, J., Berends, C., van de Berg, W. J., & van de Wal, R. S. W. (2023). Present-day mass loss rates are a precursor for West Antarctic Ice Sheet collapse. *Research Square*, *PREPRINT (*. Retrieved from `https://www.researchsquare.com/article/rs-3498111/v1` doi: https://doi.org/10.21203/rs.3.rs-3498111/v1